UNIVERSITY OF THESSALY

POLYTECHNIC SCHOOL

DEPARTMENT OF MECHANICAL ENGINEERING

LABORATORY OF MATERIALS

Diploma Thesis

« Study of High-Temperature Hydrogen Attack in carbon-steel equipment »

Volos, 2022

By

Fotaki Morfo

Submitted for the Partial Fulfillment of the requirements for

the degree of Diploma in Mechanical Engineering

ΠΑΝΕΠΙΣΤΗΜΙΟ ΘΕΣΣΑΛΙΑΣ

ΠΟΛΥΤΕΧΝΙΚΗ ΣΧΟΛΗ

ΤΜΗΜΑ ΜΗΧΑΝΟΛΟΓΩΝ ΜΗΧΑΝΙΚΩΝ

ΕΡΓΑΣΤΗΡΙΟ ΜΕΤΑΛΛΟΥΡΓΙΑΣ

Διπλωματική Εργασία

“Μελέτη στην επίθεση θερμού υδρογόνου σε εξοπλισμό από ανθρακούχο χάλυβα”

Βόλος, 2022

Από:

Φωτάκη Μόρφω

Υποβλήθηκε για τη μερική εκπλήρωση των απαιτήσεων για του πτυχίου Μηχανολόγου Μηχανικού

Certified by the members of the Thesis Committee:

First Examiner

(Supervisor) Dr. Gregory. N. Haidemenopoulos

Professor of Physical Metallurgy

Department of Mechanical Engineering

University of Thessaly

Second Examiner Dr. Helen Kamoutsi

University of Thessaly Lab Teaching Staff

Department of Mechanical Engineering

University of Thessaly

Third Examiner Dr. Kermanidis Alexis

Professor of Computational Mechanics of Structures

Department of Mechanical Engineering

University of Thessaly

Εγκρίθηκε από τα Μέλη της Τριμελούς Εξεταστικής Επιτροπής:

Πρώτος εξεταστής : Δρ. Γρηγόρης Ν. Χαϊδεμενόπουλος
(επιβλέπων) Καθηγητής Φυσικής Μεταλλουργίας
Τμήμα Μηχανολόγων Μηχανικών
Πανεπιστήμιο Θεσσαλίας

Δεύτερος εξεταστής: Δρ. Ελένη Καμούτση
Εργαστήριο Διδακτικό Προσωπικό
Τμήμα Μηχανολόγων Μηχανικών
Πανεπιστήμιο Θεσσαλίας

Τρίτος εξεταστής: Δρ. Κερμανίδης Αλέξης
Καθηγητής Υπολογιστικής Μηχανικής των Κατασκευών
Τμήμα Μηχανολόγων Μηχανικών
Πανεπιστήμιο Θεσσαλίας

Aknowledgements

This project was accomplished in the scope of the partial fulfillment of the requirements for the degree of Diploma in Mechanical Engineering at University of Thessaly.

I would first like to express my sincere appreciation to my supervisor Professor Gregory N. Haidemenopoulos, without her persistent help, the goal of this project would not have been realized.

Further, I am particularly grateful to Dr. Helen Kamoutsi and professor Kermanidis Alexis for accepting to take part in the three-member evaluation committee of my Diploma Thesis.

Ευχαριστίες

Η εργασία αυτή εκπονήθηκε στο πλαίσιο της μερικής εκπλήρωσης των απαιτήσεων για την απόκτηση διπλώματος Μηχανολόγου Μηχανικού στο Πανεπιστήμιο Θεσσαλίας.

Αρχικά θα ήθελα να εκφράσω την ειλικρινή μου εκτίμηση στον επιβλέποντα καθηγητή μου Δρ. Γρηγόρη Ν. Χαϊδεμενόπουλο, χωρίς την επίμονη βοήθειά του, ο στόχος αυτής της εργασίας δεν θα είχε υλοποιηθεί.

Επιπλέον, είμαι ιδιαίτερα ευγνώμων στην Δρ. Ελένη Καμούτση και τον Δρ. Κερμανίδη Αλέξη για την αποδοχή τους να συμμετάσχουν στην τριμελή επιτροπή αξιολόγησης της Διπλωματικής μου Εργασίας.

Study of High-Temperature Hydrogen Attack in carbon-steel

Abstract

High-temperature hydrogen attack is a common failure in petroleum refineries and petrochemical plants since the 30s and 40s. It is often encountered in equipment fabricated from carbon steel and some alloy steels. HTHA has been a cause of severe equipment damage and rarely life loss, like the tragic explosion at the Tesoro Anacortes Refinery in 2010, where seven people lost their lives. Unfortunately, the reason behind this kind of accident may be the lack of consistency in data concerning the morphology of the critical early stages and expansion of the phenomenon. Therefore, this metallographic study of a failed equipment piece -from HELPE (Hellenic Petroleum group)- aims to shed light on the processes during early stages until final failure of a material due to HTHA. Gathering information from previous studies of the phenomenon and the current metallographic study aims to help better understand the mechanism and thus, predict and reduce the likelihood of its occurrence.

Μελέτη προσβολής ανθρακοχάλυβα από υδρογόνο σε υψηλές θερμοκρασίες

Περίληψη

Η προσβολή από υδρογόνο σε υψηλές θερμοκρασίες είναι μια συνηθισμένη μορφή αστοχίας στα διυλιστήρια πετρελαίου και στις πετροχημικές εγκαταστάσεις από τις δεκαετίες του 30 και του 40. Παρατηρείται συχνά σε εξοπλισμό κατασκευασμένο από ανθρακούχο χάλυβα και ορισμένους κραματωμένους χάλυβες. Το HTHA έχει αποτελέσει αιτία σοβαρών ζημιών στον εξοπλισμό καθώς και απώλεια ανθρώπινων ζωών σε σπάνιες περιπτώσεις, όπως η τραγική έκρηξη στο διυλιστήριο Tesoro Anacortes το 2010, όπου επτά άνθρωποι έχασαν τη ζωή τους. Δυστυχώς, ο λόγος πίσω από αυτού του είδους τα ατυχήματα μπορεί να είναι η έλλειψη συνοχής των πληροφοριών σχετικά με τη μορφολογία των πρώτων σταδίων του φαινομένου και συνεπώς την αναγνώριση του. Ως εκ τούτου, αυτή η μεταλλογραφική μελέτη ενός προσβεβλημένου τεμαχίου εξοπλισμού -από τα ΕΛΠΕ (Ελληνικός Όμιλος Πετρελαίου)- έχει ως στόχο να παρουσιάσει την ανάπτυξη αυτού του μηχανισμού, επίθεσης θερμού υδρογόνου, και των σταδίων που ακολουθεί. Η συγκέντρωση πληροφορίων από προηγούμενες μελέτες του φαινομένου και η τωρινή μεταλλογραφική μελέτη στοχεύουν να βοηθήσουν στην καλύτερη κατανόηση του μηχανισμού και συνεπώς την πρόβλεψη και μείωση της πιθανότητας εμφάνισής του.

Contents

9.

Table of figures

Table of tables

Abbreviations

HTHA	High Temperature Hydrogen Attack
BM	Base Metal
HAZ	Heat Affected Zone
API	American Petroleum Institute
SEM	Scanning Electron Microscopy
TEM	Transmission Electron Microscopy
HE	Hydrogen Embrittlement
PWHT	Post Weld Heat Treatment
CSB	U.S. Chemical Safety and Hazard Investigation Board
NDE	Non-Destructive Evaluation
UT	Ultrasonic Techniques

PAUT	Phased Array Ultrasonic Techniques
TOFD	Time Of Flight Diffraction
TFM	Total Focusing Method
AUBT	Advanced Ultrasonic Backscatter Technique
WFMT	Wet Fluorescent Magnetic Particle
AET	Advanced Invasion Technique
IOW	Integrity Operating Window

1. Introduction

The document includes a literature review collecting information about the conditions that enhance the appearance of HTHA from various case studies and standard manuals, such as the API 941 (2008). The thesis gathers information of the microstructural studies of the HTHA phenomenon, in order to understand the stages that take place until equipment failure and the variables that influence its continuation. Following the general information, a section is dedicated to the preventing and monitoring HTHA methods and the evaluation techniques that can be used to examine possibly affected equipment without destroying it.

In the present thesis, there is also the investigation of the failed heat exchanger (M-9210), from the Aspropyrgos Refinery. The failure is attributed to the High Temperature Hydrogen Attack damage mechanism. Through the metallographic study and hardness measurement the thesis will add insight on the physical process that occur during the initiation and propagation of this particular case of failure. Finally, the gathered information and the results of the specimen examination will be discussed.

The heat exchanger, under study, is made of carbon-steel, ASTM A285. During service, a steam leak from the outer carbon-steel tube of the exchanger, was observed [1]. The leak occurred due to a crack on the tube's internal surface, which propagated to the external surface. HELPE sent the damaged part of the tube to the Laboratory of Materials, part of the University if Thessaly, to examine the damage and report the results.

2. Literature review

2.1 Definition of HTHA

HTHA is a permanent and irreversible microstructure failure, mostly met on equipment constructed from carbon-steel or some alloy steels, operating in hydrogen rich environment under elevated pressure. It concerns the deterioration of the mechanical properties and appears in the form of blistering, followed by fissuring until final cracking of the material.

2.1.1 Affected industries and introduction to the Nelson Curves

It is a major concern for petroleum refineries and petrochemical plants which use steel-based materials, alloyed or not. Some examples of procedures where carbon steel and alloy steels are used are the production of ammonia, oil refinement, conversion of coal, by liquefaction or gasification, and the creation of methanol. It is a common failure because equipment, used for the aforementioned procedures, often operates within temperatures and pressures that enhance the chances of hydrogen attack appearance. It results to the early replacement of equipment due to final failure and rarely to catastrophic explosions and loss of human life, such as the Tesoro Anacortes incident in April of 2010.

Carbon steel is commonly used in various equipment parts of petroleum refineries due to its availability and affordability. However, it is highly susceptible to HTHA when exposed to a hydrogen partial pressure environment higher than that of 0.48 MPa and at elevated temperatures greater than 232°C [2] . Carbon composed steels and C-Mo are the most susceptible to HTHA. However, highly alloyed steels, with Cr and Mo, offer better resistivity. In opposition, highly alloyed steels, are defective in other aspects, like the quality of welds [3] . They are also pricier.

To inform industries of the correct material selection and to specify safe operating temperatures and hydrogen partial pressures Nelson created, in collaboration with Shell oil gas company, in 1959, the Nelson Curves. These curves present HTHA favorable temperatures and hydrogen partial pressures for different materials. They are included in the API 941 manual for safe operation, a recommended Practice on “Steels for Hydrogen Service at Elevated Temperature and Pressure in Petroleum Refineries and Petrochemical

Plants". The curves were evaluated in the case of examined accidents information and new diagrams were published in the next API publications. The Nelson curves were formed based on empirical data from HTHA failures. The data for the creation and evaluation were collected through satisfactory and unsatisfactory equipment operation. While the curves are widely used, damage still occurs due to the HTHA phenomenon despite material operating within the safe limits, set by the curves. Thus, there is confusion around the conditions under which phenomenon appears.

Even though this phenomenon was discovered during the early 30s, it piques the interest of many researchers until now. Accidents and failures continuously occur because of the various aspects under which this mechanism appears and haven't been sufficiently taken under consideration.

2.2 General information about HTHA

HTHA is caused when carbon steel and some alloyed steels are exposed to an environment containing atomic hydrogen (H+) at high temperatures and pressures for a specific amount of time [4]. The mechanisms appears usually over 0.48 MPa hydrogen partial pressure and 232°C [2]. The H_2 of the environment dissociates into monoatomic hydrogen H+. Under these conditions, the hydrogen atoms come in contact with the carbon containing steel and form dissoluble gases that escape to the surrounding environment or diffuse into the interior of the metal and react with the contained carbon, to form methane (CH_4) molecules [5]. The dissolution of cementite carbides, contained inside the material, continuously provides free carbon, until their depletion. The chemical equations for the dissolution of cementite carbides are the following [2],[6]:

$$Fe_3C \rightarrow 3Fe + C$$

$$4H + Fe_3C \rightarrow 3Fe + CH_4$$

The reaction describing hydrogen molecule dissolution and methane creation is [2]:

$$H_2 \rightarrow 2H \text{ and } C + 4H \rightarrow CH_4$$

Due to their larger size, the methane molecules cannot diffuse into the material and thus accumulate, creating high-pressure methane bubbles, at the grain boundaries, inclusions,

and free surfaces, in general in the regions of high interfacial energy. However, the internal methane pressure of these bubbles doesn't exceed the pressure created by opposing surface-tension forces, and thus, the bubbles cannot be larger than the size of a nucleus [7]. Over time, these bubbles continue to form and coalesce to fissures/microcracks at the spots described above. This procedure is named HTHA «incipient attack». The final step, that leads to ultimate failure, involves the union of the countless micro-cracks into large cracks. In the final stage of HTHA, the fissures and microcracks join to form significant cracks, which lead to the final failure of the material.

2.3 Modeling

Modeling the mechanism helps understand the time dependency of the attack and establish a kinetic analysis, as well as identifying the rate controlling steps of the attack. Many researchers tried to develop models to precisely predict HTHA. Through them they proposed various main rate controlling forces of the attack.

The leading driving forces for HTHA damage initiation and development are hydrogen diffusion and reaction with carbon to form methane according to Shih and Johnson, in 1982 [8] . They studied the Nelson curve for carbon steel based on a void growth model, which included methane formation kinetics and grain boundary diffusion. They concluded that the extent of the damage to hydrogen attack depends on the material's hydrogen diffusion rate. As the level of hydrogen grows, so does the percentage of intergranular fractures, due to methane filles void coalescence. That is why a hydrogen attack can also be considered a hydrogen diffusion-controlled degradation process. The diffusivity of hydrogen, in different kinds of steel, is displayed in the picture below. Specifically, ferritic steels (**α-iron**), such as carbon steel, have a higher diffusivity than austenitic steels (**γ-iron**) (Figure 1).

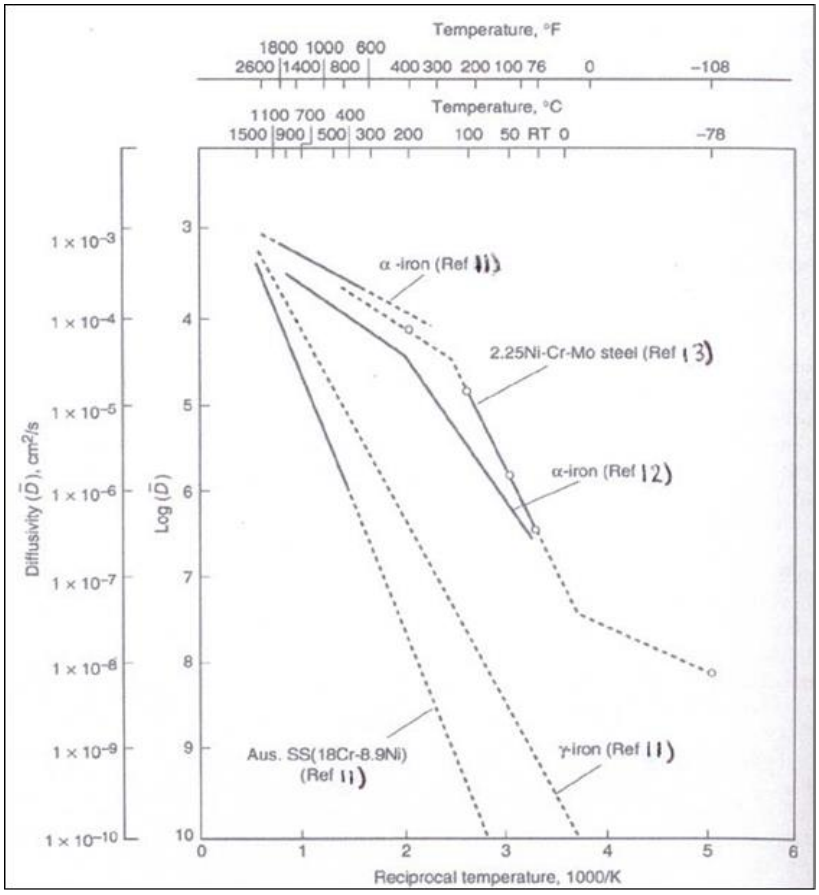

Figure 1. Diffusivity of hydrogen in various steels.

Weiner, in another study, proposes carbide dissolution as the rate-controlling mechanism for the incubation stage in synergy with hydrogen embrittlement. Thygeson and Molstad proposed the chemical reaction of methane formation as the rate-controlling factor. Shewmon concluded that the rate-controlling factor for fissure creation during the incubation stage under high temperatures is the methane bubble nucleation and expansion. As for lower temperatures, he believed the carbon supply is the rate-controlling mechanism. The depth of the attack was proposed by Bisaro and Geiger to be a function of hydrogen partial pressure squared. The hydrogen penetration rate is time dependent and increases with the passage of time as a function of temperature [9] .

In 1978, Sagues et al. employed kinetic equations to model methane production and cavity expansion via creep or grain-boundary diffusion. The growth mechanism was discovered to be temperature and methane pressure dependent. Furthermore, they discovered that the two processes controlling the damage rate are the methane formation rate, through surface reactions between carbon and hydrogen, and bubble growth due to creep. Sites close to the surface, exposed to hydrogen-rich environment, show higher rates on nucleation of methane bubbles, due to higher hydrogen pressure at this side. High hydrogen partial pressure increases internal decarburization and fissuring, increases hydrogen solubility in the material and provides a greater driving force for the attack [9] . Hydrogen partial pressure and methane pressure are linked through a quadratic equation which is:

$$P_{CH_4} = \frac{P_{H_2}}{K}$$

In this equation K is the equilibrium constant of the reaction. Thus, doubling the hydrogen partial pressure leads to a four-time increase in methane pressure and a four-time lifetime drop of the material, according to Prager [9].

All modeling attempts used a specific equation for deformation during the incubation stage strain rate:

$$\varepsilon = C\ P_{CH_4}^{n} \exp(-\frac{Q}{RT})$$

The n value was experimentally determined, using dilatometry, and indicates the growth mechanism taking place. It is n=1-2 for grain boundary diffusion, n=2-7 for bubble surface diffusion and n=7-10 for dislocation creep [9].

The attacks main rate controlling mechanisms, that derived from the aforementioned research, are the hydrogen diffusion and its reaction with dissolved carbon, provided by carbide dissolution, to form methane [10] .

The HTHA damage evolution rate versus time curves show that the damage rate constantly grows with increasing time until it reaches a maximum value, then progressively falls until it reaches zero at the end of the HTHA damage evolution process [11]. The time corresponding to maximal damage evolution was determined to be almost halfway through the HTHA damage process in most cases during the incipient attack stage, bubble formation, and early saturation stage, in which fissure creation takes place and mechanical properties are degraded. This pattern was linked to carbide exhaustion as damage evolved, resulting in decreased damage rates at intervals beyond the time corresponding to the maximum damage rate.

2.3 Mechanisms and stages of HTHA

HTHA begins with the diffusion and dissolution of hydrogen in steels. Following is the nucleation and growth of the methane filled small blisters because of reaction of hydrogen with carbon, from dissolved carbides [9]. In carbon steels , that consist of a ferrite and pearlite matrix the damage appears more often with the nucleation and growth of bubbles on ferrite-pearlite grain boundaries, as pearlite is the usual carbon source for this mechanism [12]. In this chapter, firstly, are presented the mechanisms that make up the HTHA damage and then the mechanisms that collaborate with hydrogen attack and affect the expansion of the phenomenon.

2.3.1 Hydrogen Solubility and Diffusion

When steel equipment is exposed to hydrogen rich environment under high temperature and high hydrogen pressure, hydrogen is absorbed and dissolved into the material. The equation informing which is the maximum amount of hydrogen that can dissolve in the steel is Sievert's law [6]:

$$C_H = kP_{H_2}^{1/2}$$

In the equation A is a constant, P_{H_2} is the hydrogen partial pressure, and Q is an activation energy. The solubility of hydrogen increases with increasing temperature, and even more with the synergy of high pressures [13],(Figure 2).

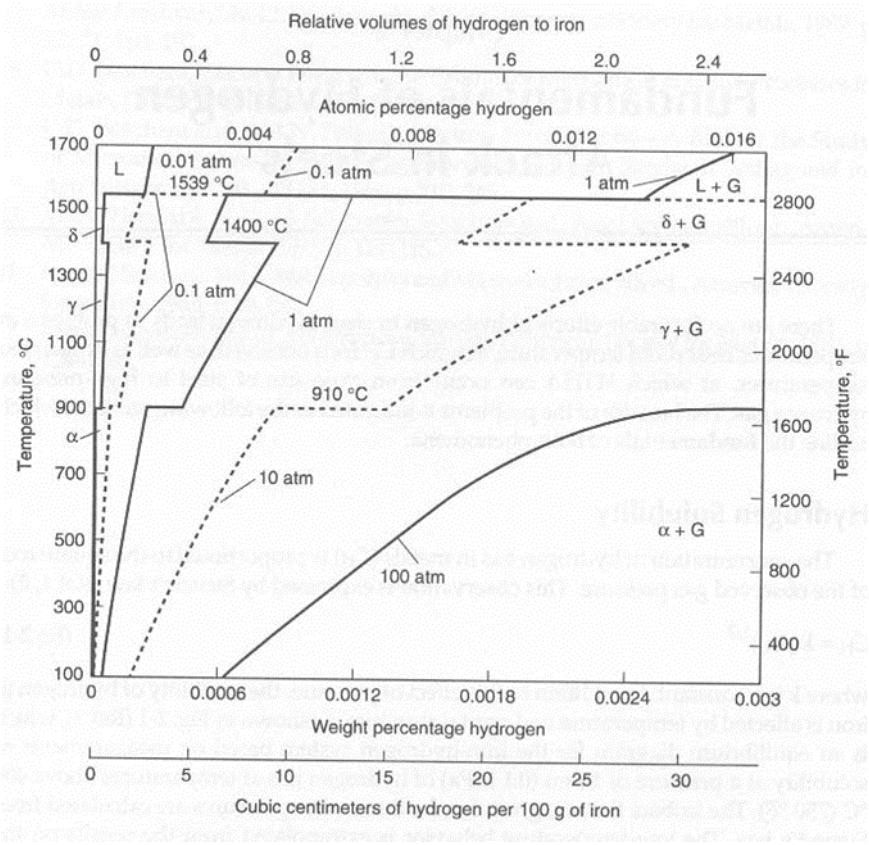

Figure 2. Hydrogen Solubility Curves.

Hydrogen diffusion away from the internal surface of the material follows absorption and dissolution. Hydrogen diffusion is required for the apparition of hydrogen attack. Without the diffusion the creation of methane is impossible, since there is no reaction with the carbon in the material. Diffusivity (D) of hydrogen in the material is described by the following equation [2]:

$$D = A_D e^{-Q_D/RT}$$

2.3.2 Decarburization

Decarburization is a high-temperature damage mechanism that occurs in carbon or low-alloy steels. It is the reaction of the free carbon and the diffused monoatomic hydrogen in the steel (loss of carbon) to form insoluble gasses. Cementite carbides (Fe_3C) dissolve to provide free carbon [14]. During this damage mechanism occurs a reduction of the material's strength and hardness, due to the dissolution of cementite, which is responsible for strength increase of the material. Carbon steel with a higher composition in carbon, included in the cementite carbides, shows higher mechanical strength.

The decarburization procedure is divided into the following two categories [2] :

• Surface decarburization.

• Internal decarburization and cracking.

2.3.1.1 Surface decarburization

It occurs on the surface of equipment that is in contact with hydrogen. It usually develops at temperatures higher than 232^{o}C combined with low partial pressures of hydrogen, lower than 0.48 MPa [2]. Carbon diffuses to the surface of the equipment to form gasses like CO and CO_2 due to the reaction with hydrogen in the operating environment. As a result, there is a continuous supply of carbon to the surface to restore thermodynamic equilibrium. The consequence of this process is the decarburization of the steel equipment. Because everything happens at the material's surface, there is no significant reduction in strength [15].

2.3.1.2 Internal decarburization and cracking

Internal decarburization along with methane bubble formation are the main HTHA damage causes. It occurs mostly at low temperatures, but not lower than 221^{o}C, in combination with high partial pressures of hydrogen, higher than 0,48 MPa [2]. This procedure arises from the atomic hydrogen, which diffuses into the carbon-steel equipment, and reacts with the carbon present as either interstitial carbon or in the form of carbides. The reaction results to methane bubble formation. Due to their large size, methane molecules cannot diffuse out of the metal and thus are concentrated at the grain boundaries, inclusions, or free surfaces.

The continuous formation and accumulation of the bubbles result in their fusion. Together with the simultaneous development of high internal stresses bubble fusion results in fissuring of intergranular character. Carbon loss to methane is the internal decarburization of steel, through carbon loss to methane formation, the mechanical properties change, for example reduction in strength and hardness becomes evident. It can cause much more serious damage than surface decarburization, since the interior of the material is affected [9].

2.3.1.3 Blistering

Many researchers recognize blistering as a third form of hydrogen attack. The build-up of molecular gases causes blistering, primarily by accumulation of hydrogen and methane gasses, on the top of the crack tip or on flat interfaces close to the interior surface, for example on grain boundaries. The blistering mechanism's morphology has been proposed by M.L. Martin, M. Dadfarnia, S. Orwig, D. Moore and P. Sofronis, as far as grain cavitation is not yet widespread [12]:

- Methane is created in-between the matrix interfaces or inside inclusions.
- Methane pressure builds up inside this newly created space, and bubbles/blisters are formed along the grain boundaries/interfaces.
- Methane pressure leads to the creation of more bubbles and the expansion of the existing ones on crack tips or near hydrogen rich environments.
- Cracks form and grow by the subsequent coalescence of the bubbles.

2.3.3 Synergy mechanisms with HTHA

2.3.3.1 Hydrogen Embrittlement

Hydrogen embrittlement is a reversible damage common in refineries that use hydrogen for improving product quality. Hydrogen in the material lowers the strain rate, which is required for cracks to form and expand. Materials in temperatures over 150 °C are immune to this mechanism. It occurs when atomic hydrogen diffuses into a material's high residual or applied stress regions and results in embrittlement and loss of ductility [16]. It also results in loss of tensile strength and the creation of sub-critical cracks. It may occur upon cooling of the equipment, due to the insufficient removal of hydrogen from the interior.

Moreover, moderate stresses assist the mechanism. As the strain rate lowers, the effect of hydrogen on fracture characteristics increases. While an increase in stress, lowers the effect of this mechanism on the material, and different mechanisms cause a fracture. In combination with residual stresses, this mechanism is irreversible damage that causes

degradation of the mechanical properties. The combination of HE and fissures in a welded area, where high residual stresses are present, can cause severe failure by cracking [16] .

Higher-strength materials are more susceptible to this type of damage mechanism. As the strength, of these steels, increases fracture toughness and the possibility of hydrogen induced cracking. To avoid it the material should be cooled for some time in between 200°C and 300°C for dissolved hydrogen to diffuse to the exterior. Post Weld Heat Treatment diminishes the existence of stresses but does not annihilate them. Older equipment is highly susceptible to this kind of damage, possibly because older material are mainly carbon steels. Multiple types of damage that depend on the composition, manufacturing, and environment are covered by the term HE.

2.3.3.2 Creep

Creep and HTHA have been proved to have essential similarities, and many researchers discovered the synergy of these mechanisms under specific conditions. Synergy has been presented under low pressures and high temperatures. Creep is the deformation of the material under moderate and sustained stress in an environment of 40%-50% T_m, where T_m is the melting temperature of the material [9]. The temperature at which carbon steel is affected by creep is approximately 345°C. Researchers have stated that creep facilitates bubble growth [17]. Creep also, aids the expansion of intergranular voids and fissures that later develop into micro cracks and lastly macrocracks. Even though creep doesn't cause the final failure of the equipment, it appears as an enhancing mechanism of crack propagation on the crack tip and methane bubble expansion [9], [12].

2.3.3 Stages of HTHA development

Many researchers have categorized HTHA in various ways according to the number of stages. Categorization recognized by many researchers depends on the change in mechanical properties.

For carbon steel at various temperatures and hydrogen pressures, Weiner [9] produced experimental curves of HTHA damage percent versus time of exposure and identified four stages of attack (Figure 3). The stages were separated as follows:

1. **Incubation.** During this stage the deterioration of the mechanical properties is undetectable.

2. **Rapid attack.** In this stage there is serious damage of the mechanical properties.

3. **Transition.** During this stage a slight decrease in the deterioration of the mechanical properties is observed.

4. **Steady state**. The rate of deterioration is now low.

According to Weiner, an augmentation in temperature or hydrogen partial pressure causes the curve to shift to shorter durations, shortening the time length of the incubation stage (Figure 3), as indicated by the dotted curve.

The four stages were officially recognized by the API 941 in the 8th edition, in 2016.

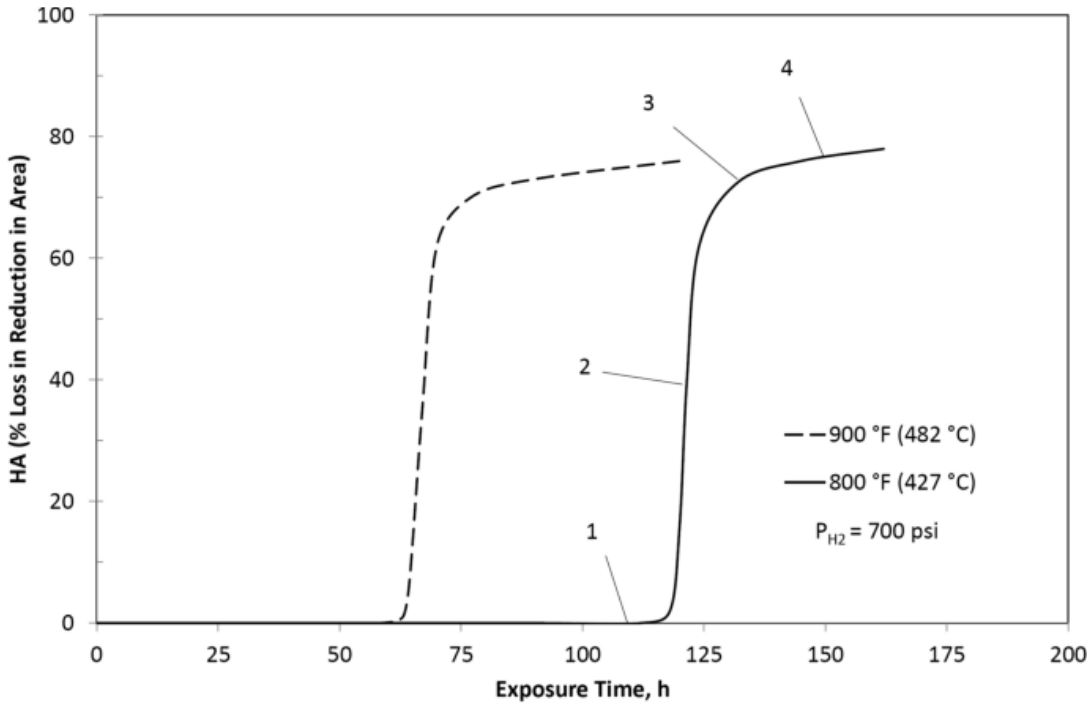

Figure 3.The curve Weiner proposed, showing also the 4 stages of attack.

According to studies by Vitovec, Vagarali et al., HTHA occurs in three stages, ignoring the transition stage [9]. The basic three stages were also recognized by the API 941 (6th edition, 2004). The stages are [2]:

• Incubation stage (Induction period, reversible loss in ductility).

• Rapid attack stage (irreversible softening due to increasing decarburization).

• Saturation stage (intergranular fissuring, irreversible embrittlement).

Incubation stage

During the incubation stage, methane bubbles are formed at grain boundaries, triple points, and inclusions. Swelling in this attack stage is immediate upon the material's exposure to favorable HTHA conditions but progresses slowly [15]. These methane-filled voids grow slowly during incubation due to the internal methane pressure and applied stresses. The duration of the incubation period depends on the temperature and decreases with temperature increase. It depends, also on the rest of the operating conditions and the composition of the material, to be more specific carbon content and the presence of alloying elements. It can be perceived exclusively using SEM (Scanning Electron Microscopy) and TEM (Transmission Electron Microscopy). The general belief that there is no attack during the incubation period stems from the fact that voids in the early stages of an attack are the size of a nucleus and go unnoticed by even the most advanced optical microscopic techniques. Mechanical properties also, remain unchanged, making it even harder to detect.

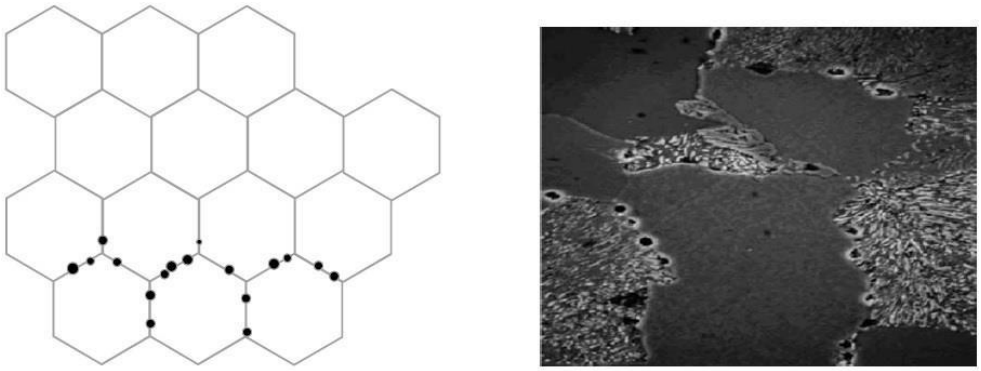

Figure 4. Creation of methane bubbles on critical points.

It occurs for the longest part of the lifetime of the equipment. Incubation period length is crucial because it determines the useful life of steel under conditions in which HTHA occurs. Incubation curves (Figure 5) are provided in the API and can be used as a measure to determine approximately safe operating times for carbon steel equipment, non-welded or welded and heat treated.

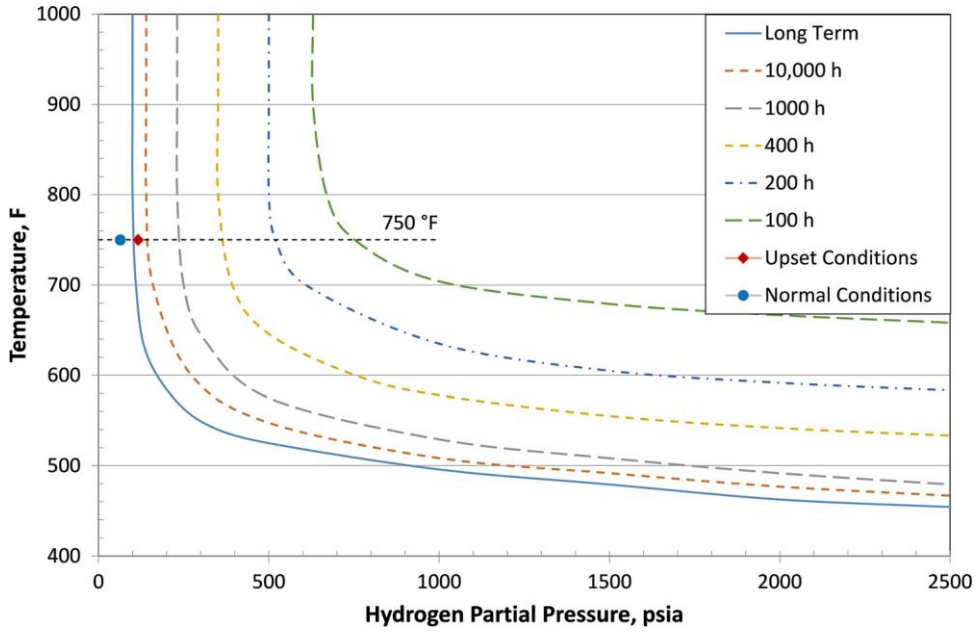

Figure 5. Incubation curves for carbon steel, not welded and welded and heat treated.

HTHA incubation times have been calculated for plain carbon steel according to the following equation [6]:

$$t_i = C P_E^{-n} \, exp[\frac{Q}{RT}]$$

In this equation C = constant = 1.39X106, P_E = exposure pressure (psi), n = constant = 3, Q = activation energy = 14.6 (kcal/mol) and T = absolute temperature.

Weiner proposed this equation through experimental procedures and by combining two equations, one for incubation time and temperature and one for incubation time and pressure. Results should always be compared with reported service failures to assure adequate agreement.

Rapid Attack stage

Methane bubbles coalesce, and small fissures form along the grain boundaries and critical points of bubble creation. In addition, internal decarburization is observed. Thus, there is alternation of the mechanical properties of the material. The hardness and strength of the metal decrease. HTHA is usually detected in this stage of attack.

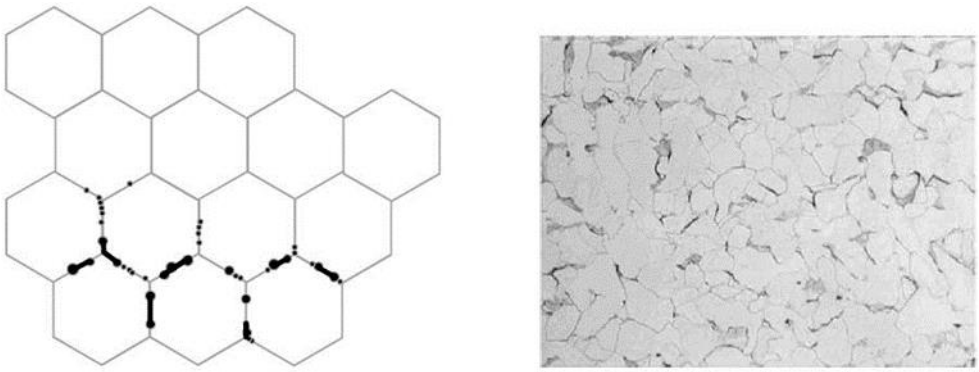

Figure 6. Creation of fissures through bubble coalescence.

Saturation stage

The crack has reached the end point of failure for two possible reasons [18] :

1. Due to micro-cracks joining into larger cracks allowing leakage from the inside of the equipment during operation. This phenomenon can take years to appear.

2. Due to abrupt separation of the metal because of its reduced strength and hardness.

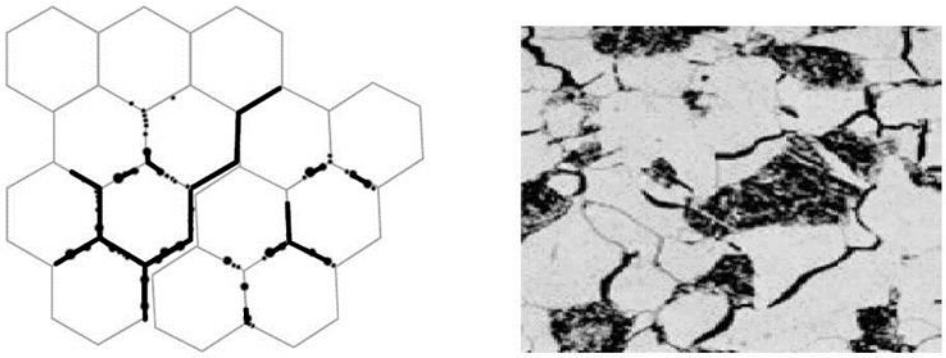

Figure 7. Linking of fissures into macro-cracks. Severe damage observed.

It should be noted that the first two stages depend on the temperature variable, whereas the last stage is little affected by it [19].

Vitovec, in 1982 [9], proposed classifications, which were not based on the mechanical properties of the material. He proposed one concerning the kinetic analysis of HTHA.

In the kinetic analysis and physical reaction model he showed that methane formation is following these eight stages:

Stage 1: Hydrogen molecules (H_2) adsorb on the metal surface.

Stage 2: The H_2 molecules dissolve and dissociate to hydrogen atoms (H+) on the surface.

Stage 3: The H+ diffuse to the critical sites where reactions can take place.

Stage 4: The cementite carbon containing carbides dissolve and provide free carbon.

Stage 5: The free carbon diffuses to the critical reaction site where the atomic hydrogen is.

Stage 6: Hydrogen on the site of the reaction reforms into H_2 molecules.

Stage 7: Carbon adsorbs on the reaction site and the hydrogen molecules.

Stage 8: Hydrogen molecules react with the carbon and form methane molecules on the site.

In the picture below is displayed a different mechanism which is based on the chemo-physical reactions that happen during HTHA.

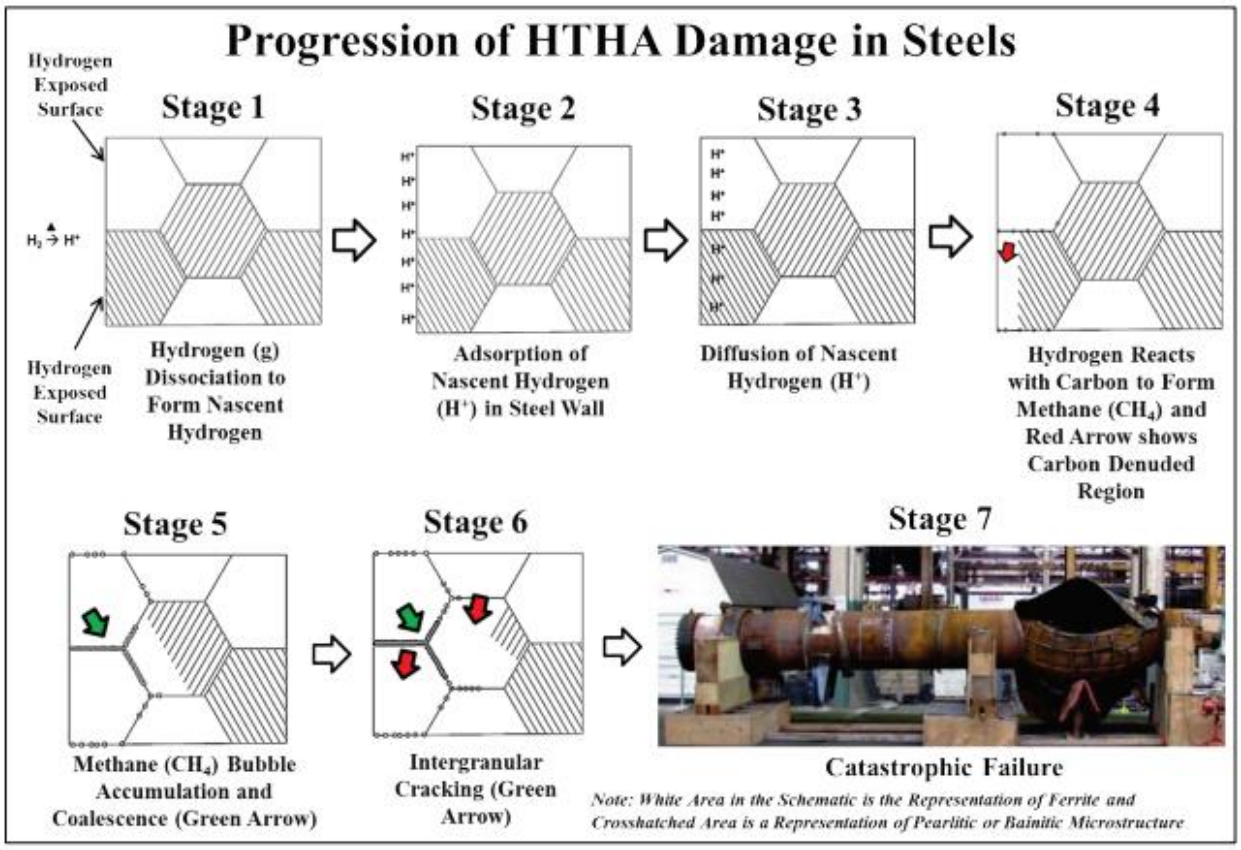

Figure 8. Seven stages of attack.

2.3.4 Phases of carbon steel and alloys used in petroleum refineries

Steels used in petroleum refineries are either ferritic or martensitic steels. Depending on the carbon content of the material, steels develop different microstructures. Steels containing 0,08% wt. carbon up to 0,12% wt. develop a ferritic microstructure. Ferritic steels can also contain chromium up to 30% wt. Another category of steel is the martensitic one. Martensitic steels contain carbon within the range of 0,1-0,25% wt. and chromium in approximately 10%-18% wt. Martensitic steels display much higher mechanical strength and hardness [20]. They have proven to be, using empirical methods, less susceptible to HTHA than carbon steel and C-0.5Mo steel, in accordance also with the Nelson Curves, but are very challenging to weld [3].

The reason that martensitic steels are challenging to weld, is the creation of non-immigrant martensite. In addition to the previous malfunction, a total hydrogen absence is required during the welding. Under hydrogen presence, S and Se contained in the martensitic materials create gases, and the weld becomes porous.

Material selection, thus, is a serious matter and careful consideration of all variables is complicated but necessary.

Ferrite (α)

Ferrite is formed during the slow cooling of hypereutectoid steel [20]. Austenite (γ) is transformed to ferrite between the A3 and A1 temperatures. Ferrite can also be created by the sudden cooling of austenite below the A1 temperature but higher than 600° C. The material must remain at this temperature until austenite is changed into ferrite. The transformation is diffusive and begins with the nucleation and growth of the ferrite phase.

There are three ferrite categories:

- Grain-boundary ferrite.
- Widmanstätten ferrite.
- Intergranular ferrite.

Grain-boundary ferrite consists of crystals that nucleate and grow on the austenite grain boundaries under an approximately 800° C temperature.

Widmanstätten ferrite is formed in lower temperatures than grain-boundary ferrite in the shape of microscopic tiles.

Intergranular ferrite consists of ferrite crystals that form inside the austenite grains in lower temperatures that the Widmanstätten ferrite.

Pearlite (P)

During the cooling of austenite below the eutectoid temperature (A1), pearlite is formed according to the eutectoid reaction:

$$\gamma \rightarrow \alpha + Fe_3C$$

In its morphology, pearlite exhibits a lamellar structure formed by the superimposition of ferrite and cementite plates. Pearlite is a mix of the continuous ferrite phase and cementite carbides. The pearlitic transformation is diffusive and takes place by nucleation and growth of the pearlitic matrix. These different phases develop during the heat treatment processes of the steel, to be more specific during the cooling procedure of steels from the austenitic phase [20].

Cementite (Fe3C)

Cementite contained within the perlite matrix is not thermodynamically stable, and its free energy of formation is more than zero. As a result, the pressure exerted in the region of cementite by methane formation is greater than it would be if carbon was in a solid solution contained in more stable carbides or even graphite. Cementite is the least stable carbide in a material responsible for the resistance to hydrogen attack of carbon steel [13]. When cementite is alloyed with molybdenum, chromium, or other soluble carbide formers, the free energy of methane generation is lowered. The free energy of methane generation and carbon activity is reduced depending on the degree of enrichment with the elements listed above.

Furthermore, the crack propagation due to the cementite carbides is enhanced because very high methane pressures are expected in the presence of cementite, even at low hydrogen partial pressures. Cementite carbides have a higher consistency in carbon.

Martensite

Martensite is a non-diffusive phase transformation [20] . It is created by the rapid cooling (quenching) of austenite of carbon steels. The cooling rate is high enough to prevent the diffusion of carbon out of the matrix, preventing, thus, cementite carbide forming. It is created by the movement of glissile interfaces. These surfaces are composed of arrays of linear dislocations, the sliding of which causes the movement of these interfaces without the need for atomic diffusion. It is in the form of plates or laths. Martensite offers to the steel very high mechanical strength and hardness, especially due to usual combination with other chemical elements, like Chromium and Molybdenum. Unfortunately, after quenching it becomes brittle. As a result, tempering takes place. During tempering, the martensitic material undergoes aging, which enables cementite precipitation. The materials harness decreases but ductility increases.

Carbon steel depending on its carbon content, is divided into three categories [20]:

- Hypoeutectoid (%C<0.8)

- Eutectoid (%C=0.8)
- Hypereutectoid (%C>0.8)

The carbon concentration controls the phase transformation.

Plotting the phase diagram reveals the composition of the metal at various temperatures (Figure 9).

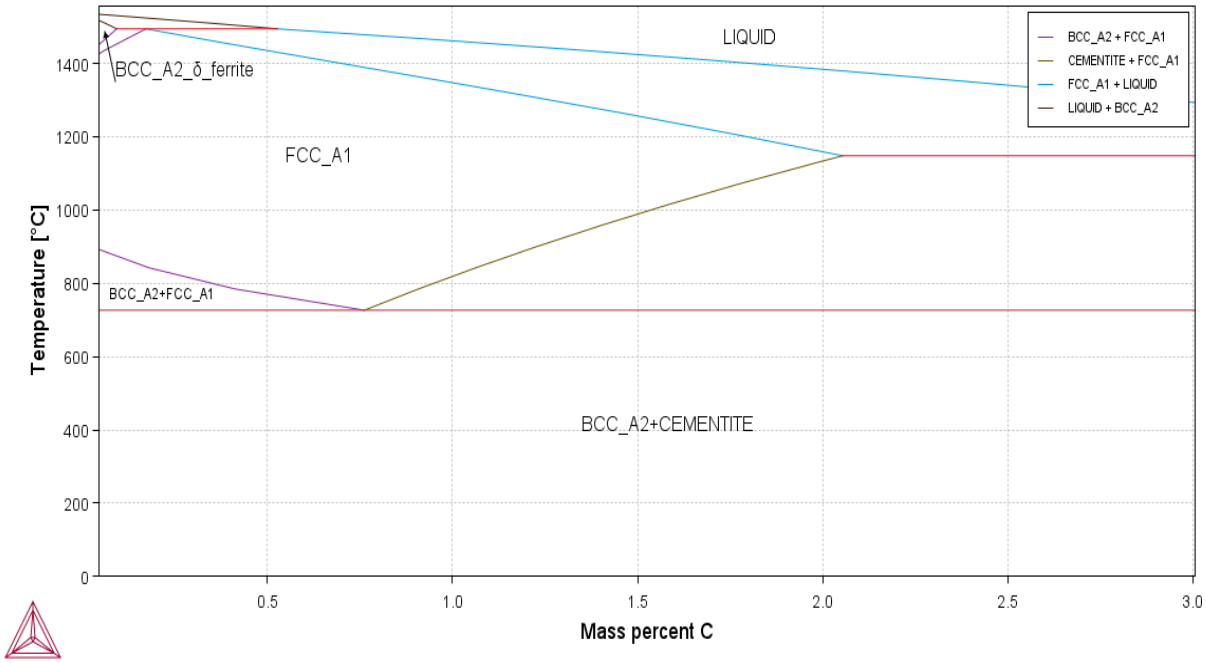

Figure 9. Phase diagram for carbon steel.

2.4 Effects of hydrogen pressure, temperature, stress, exposure time, affected materials, and the affected equipment

Hydrogen attack depends mainly on the temperature, on partial hydrogen pressure, on time of exposure of the material and the composition and structure of the steel [13]. Other variables, such as heat treatment, surface condition, and stress also affect the HTHA mechanism propagation, but are insufficient for its creation.

- **Temperature**

High temperatures accelerate the speed and severity of the attack. The increase in temperature facilitates the diffusion of carbon and the rate of carbide solution. High temperatures favor external decarburization because of the carbon diffusion to the surface,

while low temperatures restrict carbon diffusion, and thus, internal attack occurs. Even an increase of 25°C can damage the material [9]. The limiting temperature for each material depends on its composition. For carbon steel HTHA is possible to appear over 200°C. Increase in temperature also increases the hydrogen dissolution and diffusion rate.

- **Hydrogen Partial Pressure**

Hydrogen partial pressure also affects the severity and speed of the attack. Under high pressure, the temperature over which steel is affected by HTHA is much lower than the temperature required under atmospheric pressure [13]. However, hydrogen partial pressure affects the damage rate less than temperature does, for example doubling the hydrogen partial pressure can lead to moderate damage rates.

The limiting threshold of hydrogen partial pressure also depends on the composition, stress, operating temperature, and environment of the material. Researchers consider various limiting pressures for carbon steel, with 0.7 MPa being the most common one. Also, Nelson, in the curve diagram considers this the limiting hydrogen partial pressure for the carbon steel.

- **Methane Pressure**

Augmented methane pressure inside inclusions can lead to expansion of voids and coalescing in the form of micro-fissures. The methane pressure inside the voids is the result of the addition of partial equilibrium methane pressure and hydrogen partial pressure, according to the following equation [8]:

$$P_m = P_{CH_4} + P_{H_2}$$

- **Exposure time**

Temperature and hydrogen partial pressure under which the equipment operates depends on the exposure time. An increase in exposure time increases the attack propagation and lowers the operating temperature and pressure under which the equipment should operate [13]. Nelson in 1965 showed the dependance of exposure time on temperature and pressure by creating incubation period curves for carbon steel and C-Mo steels (**Error! Reference source not found.**). Apart from Nelson Curves, the “Prager curves” were created , by Panzarella and Cohran in 2016 [9], for prediction of the failure time in carbon steel and C-Mo steels.

- **Steel alloying**

Naumann discovered that alloying the material with solid carbides, such as Niobium (Nb), Zirconium (Zr), Chromium (Cr) and Molybdenum (Mo), increases the stability of cementite carbides and creates an HTHA-resistant material [8],[21]. These elements are of greater thermodynamic stability than cementite, thus offering better resistance significant. Carbide-forming alloy elements, such as Cr, Mo, V (Vanadium), Nb, and Ti (Titanium), reduce the tendency for internal fissuring due to their stabilizing influence on internal iron carbides [18]. For example, the Chromium content affects the incubation stage timewise, and an increase in chromium leads to prolonging the incubation stage and offers better resistance [13]. Carbon steel is the most sensitive material. Martensitic steels, which have a higher Cr content, show the highest resistance to HTHA, according to the Nelson Curves. Also helpful to resistivity is the reduction of elements like Sulphur (S), Silicon (Si), and Nitrogen (N) and the increase in Vanadium. According to Rosenthal, impurities that segregate at grain boundaries, such as Phosphorus and Sulphur, can slow down grain-boundary fissuring by HTHA in carbon steel. They hypothesized that the grain-boundary energy and grain-boundary diffusion reductions were what caused the retarding impact. Even small amounts of alloying elements are promising. Molybdenum is also used to increase the creep strength of the material and prevent deformation. Finally Shida et al. showed, using simulation, that an addition of Boron in Cr-Mo steels increased the resistance of the HAZ side in HTHA [15].

- **Carbon content**

The attack rate and the microstructure damage depend on the equipment material's initial carbon content. Low carbon in the chemical composition increases incubation length, whereas higher carbon content is more susceptible to attack [19],[13]. A small amount of methane is insufficient for the number of fissures and methane bubbles needed to be created for the phenomenon to be studied as HTHA.

Carbon activity measures how much carbon in the metal solution is accessible to react with hydrogen to generate methane, and it reflects the stability of the least stable carbides. Because stable carbides only react with hydrogen when dissolved, alloys containing them have lower carbon activity. Cementite is an unstable carbide for temperatures over 200°C and dissolves in a higher rate under such temperatures when hydrogen is present. This is the reason for low susceptibility of carbon steel and C-Mo steels. Fabrication techniques like welding, heat treatment techniques, like PWHT (Post Welding Heat Treatment), and tempering reduce carbon activity. As a result, various zones of a welded joint should react differently to an HTHA attack. Furthermore, heat treatment leaves the steel oversaturated with dissolved carbon. As a result, the time until the attack is reduced. High temperatures and hydrogen partial pressures are required for low carbon concentration to achieve a damaging reaction rate. According to Archakov, during preventive heat-treatment of the specimen, the rate of decarburization for pearlitic steel reduces with an increase in

tempering temperature. This rise in tempering temperature also induces an increase in the stability of the carbide phase.

High carbon content accelerates the kinetics of the reaction if all other characteristics remain stable. However, mechanical strength and hardness in carbon steel depends highly in carbon content, so its unwise to reduce carbon for HTHA prevention. Utilization of alloyed steels is much preferable [18]. Concerning the structural characteristics fine-grained structure offers better resistance than coarse-grained, for example fine-grained pearlite is preferable.

- **Stress**

Stress is an essential parameter because HTHA is forwarded by residual stresses and demands the lowering of temperature for the attack to be prevented. Stress can lead to HTHA while equipment operates in the safe zone of the Nelson curves. Residual stresses increase the crack driving force and reduce the resistance to brittle fracture [16]. Stresses enhance the creep phenomenon and cause enlargement of methane filled inclusions and grain boundary separation. In high applied stresses and moderate temperatures, fissuring can appear ahead of decarburization, as Inglis and Andrews reported in 1930. With applied stress, the HTHA incubation time decreased, and decarburization was accelerated in specimens under stress, as mentions Yokogawa [9]. HTHA can usually be found in high stressed areas, near weld heat-affected regions. Moreover, stresses can be created by continuous thermal gradients during the start-up or equipment cooling after usage, even though the equipment was operating in the “safe zone”. Sudden shutdowns, also increase the possibility of HTHA forming.

- **Material microstructure**

As far as the microstructure is concerned, larger grains are more susceptible to HTHA. Coarse weakly bound particles, creating inclusions, coarse pearlite, or other carbides provide good spots for void nucleation and methane forming initiation, due to higher diffusivity within a coarse grained structure [18]. Coarse pearlite sites are preferable for methane bubble nucleation than fine-grain pearlite. Prager [9] observed that in sites of welds, HAZ regions are more sensitive to this type of damage, and results varied for the coarse-grained and fine-grained regions. Therefore, inclusions near coarse pearlite colonies are highly possible to fill with methane.

Furthermore, the aggregation of carbides along grain boundaries increases the sensitivity of steel to HTHA. Carbides homogeneously dispersed in the matrix provide better results. Hasegawa and Nomura discovered that when the carbides were continually precipitated at the grain boundary as opposed to being uniformly dispersed in the matrix, carbon steel was more susceptible to HTHA, due to the localization of the damage [9].

The areas affected by heat treatment, for example welded regions or HAZ zones, are characterized by coarse grains and instability of the carbides. Therefore, those regions are more susceptible to HTHA.

- **Welding**

Welding can change the material's susceptibility to HTHA. It can alter the grain size, lessen the stability of carbides, such as cementite, and cause the creation of residual stresses. As a result, particularly in the HAZ side, welded components are frequently more vulnerable to HTHA [9]. PWHT is a controlled reheating process of the metal. It increases HTHA resistance. PWHT stabilizes the carbides in the material [8]. It is known that an alloy steel's HTHA resistivity, for example in C-0.5Mo or Cr-Mo steels, can decrease to that of carbon steel, if insufficient PWHT is performed. It is preferable, in PWHT, to use materials non-susceptible to HTHA, for the filler metal for example, which can have a lower carbon composition. Low hydrogen welding procedures are also advised, like GMAW welding [16].

- **Heat Treatment and Cold Working**

Heat Treatment is the controlled heating of steel in order to alternate its microstructure and configurate its properties. Heat treatment leads to an increase of the incubation time length of HTHA, by reduction of the carbon in the matrix. Especially in carbon steel, this treatment can increase the resistance of the material by five times the corresponding unit size [9]. Low-alloy steels' type and stability of carbides are influenced by tempering temperature and its duration, and this in turn affects how susceptible they are to HTHA. Heat treated steels for a longer amount of time show better resistance due to increase in ductility, strength decrease with consequent dislocation movement, which alleviates the material from residual stresses [8].

Cold working of a material increases the fissure appearance rate. Furthermore, it leads to augmented decarburization rates, as well as the carbide precipitation. Hence, the mechanical strenght of the material lowers [8].

- **Corrosion**

Corrosion can either obstruct or promote the diffusion of hydrogen. For example, the layer of corrosives on the metal surface can work as a barrier and delay the hydrogen adsorption in the interior of the equipment. A corrosion product can be viewed as an equivalent or additional cladding thickness. Corrosion in through the interaction with tensile residual stresses cause stress corrosion cracking due to toughness reduction and embrittlement [16].

Large inclusions or **residual discontinuities**, for example, low energy interfaces, provide free surfaces for methane formation or nucleation of voids and blisters. The **thickness of the equipment material** and creep strength may affect the procedure of HTHA.

2.5 Nelson curves: Background of Nelson curves and usage information

Johnson first discovered the process in 1875, through exposure of steel wires to an aqueous environment). However, most of the phenomena were observed in the 1930s and 1940s. Then empirically, in collaboration with Shell oil gas company and George Nelson, in order for equipment to operate safely, made some conclusions about HTHA through gathered empirical information which were formalized by the publication of the Nelson curves in 1949 [22]. The creation of the curves is based mainly upon industrial data of damaged and credibly operating equipment. They were derived by considering the operating temperature of the equipment and the partial pressure of hydrogen for various steel alloys, with different carbon and other alloying elements. The API (American Petroleum Institute), in collaboration with Dr. Vitovec, revised the curves in 1960. Updated versions with adjusted limits, from the original version of the curves diagram, have been issued, in more recent API publications, resulting from the study of failures, of more industrial operating equipment. The curves are used extensively by petroleum refineries as guides for the selection of proper materials and safe operating conditions [9].

The diagram shows, with dotted lines, the surface decarburization stress of the material. The continuous lines describe the tendency for internal decarburization and crack formation. The equipment used according to the composition of the metal must operate beneath the defined curve of the diagram. To be more specific, the operating conditions should not exceed the temperature and hydrogen partial pressure defined by the ends of the curve to prevent failure. Moreover, the Nelson Curves are time independent. By studying the curves, petroleum refinery staff can inform themselves about the right choice of material and its operating conditions. However, the Nelson Curves are not absolute. Equipment failure from HTHA has been reported even though the equipment was operating in safe conditions.

A significant change concerning the carbon-steel curve was made after a deadly explosion at the Tesoro Anacortes Petroleum Refinery. A carbon steel heat exchanger tube failed, despite operating within the safe limits, and exploded resulting to the death of 7 people. As a result, two curves describe carbon steel in the latest API edition. One refers to post-weld heat-treated carbon steel, and another to carbon steel lacking heat treatment. The non-heat treated one should operate under lower temperature and hydrogen partial pressure, as it is the most susceptible. The addition of this curve was also based on empirical data received from reports of carbon steel failed equipment from petrochemical plants [9].

Significant changes have been made, also, on the 0.5Mo curve. During the following years several reports of failures under the curve of 0.5Mo steel were received and raised concerns in the industry. As a result, the curve was lowered by about 30°C in the 2nd edition of API 941. As pointed out by Baumert et al., the 3rd edition of API 941 (1983) was not revised even though failure reports proved damage took place under the 0.5Mo curve. In this edition, only caution during usage in catalytic reformers is advised. The curve was removed on the 4th edition of the API 941 (1990) due to continuous unexpected failures. A separate presentation for this kind of steel was created to alarm users to be cautious when dealing with this steel [9].

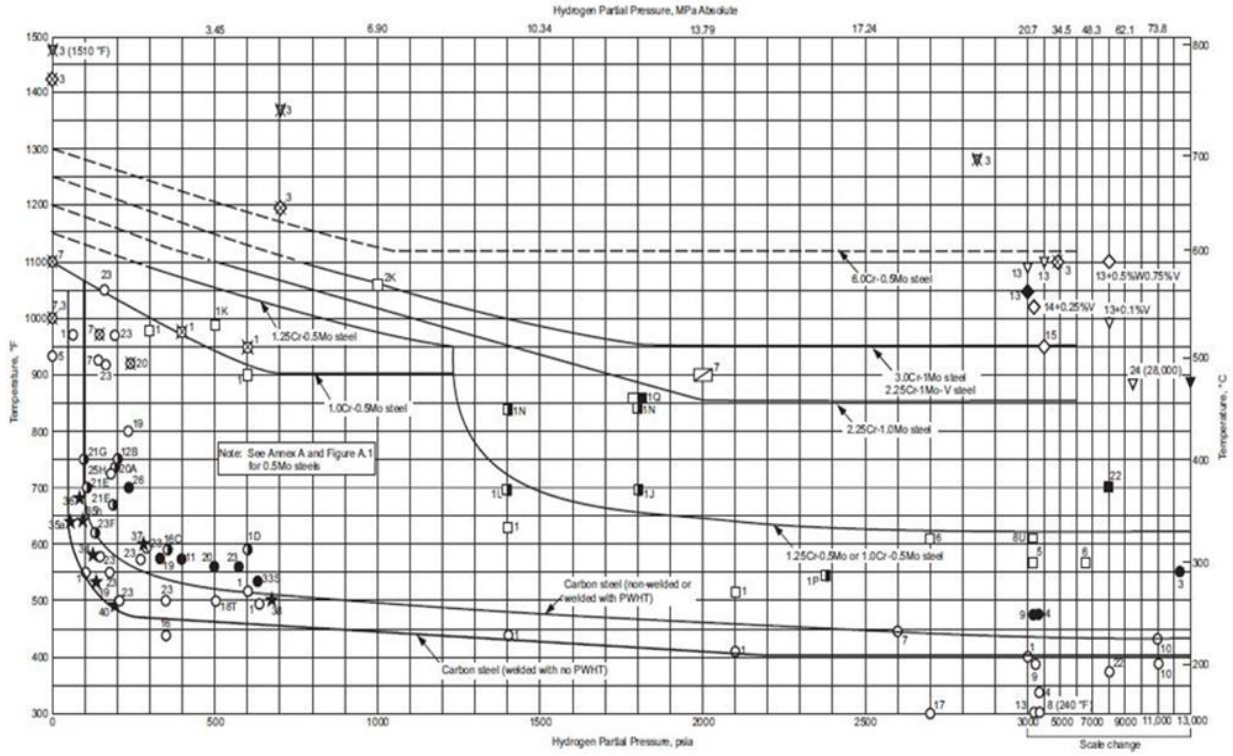

Figure 10.Nelson Curves for carbon steel and alloyed steels.

Nelson also created curves that predict the time for an incipient attack called “incubation curves” for carbon steel and 0.5Mo steel, previously presented in Figure 4. These curves show how time affects the temperature - hydrogen partial pressure curves. Practically it shows the effects of sudden unplanned increases in temperature or pressure on HTHA. These curves aid in predicting detectable HTHA occurring after an upset of the parameters described above.

Many researchers have considered Nelson curves lacking due to since they fail to conclude information about other parameters that affect HTHA, such as the time dependency of the attack and creep strain affecting the material [17] . Many accidents, also, have been reported with equipment operating beneath the limits set by the Nelson Curves. Therefore, the methodology using the curves is considered inaccurate or insufficient to predict HTHA.

Van der Burg et al. further noticed that, on the one hand, predictions for materials containing unstable carbides under high-stress levels need a more conservative approach. On the other hand, the curves for materials with stable carbides, due to proper heat treatment, under low stresses need relaxation. Other researchers have attempted to change or replace the Nelson curves. In 2016, Staats and Buchheim [9] devised a qualitative methodology for applying altered Nelson curves in risk management planning, published in 2016. The technique considers cladding type and thickness, corrosion scale, and trust in the operating information in addition to the two key factors, temperature, and pressure. Relying on the Nelson curves and the elements they would examine in each scenario, they created an "adjusted Materials HTHA Resistance curve". Each factor was evaluated to see if it would elevate or reduce the curve. The disadvantage of this strategy is that it is subjective, with no theoretical or experimental requirements. Nevertheless, they concluded that using a qualitative way to organize inspections is more feasible than attempting to calculate HTHA's remaining life, which would be time-consuming if all variables were considered. Therefore, Panzarella and Cochran, to supersede Nelson curves for "safe zone" evaluation, created time-dependent curves, also known as Prager curves. Several curves, instead of one, were presented for various periods [9]. These curves were formed using a probability approach and a Monte Carlo analysis.

After examining the accident at the Tesoro Anacortes Refinery, the U.S. Chemical Safety and Hazard Investigation Board (CSB) recommended new limits for the operating characteristics of carbon-steel equipment such as 0,3447 MPa and 204,44° C.

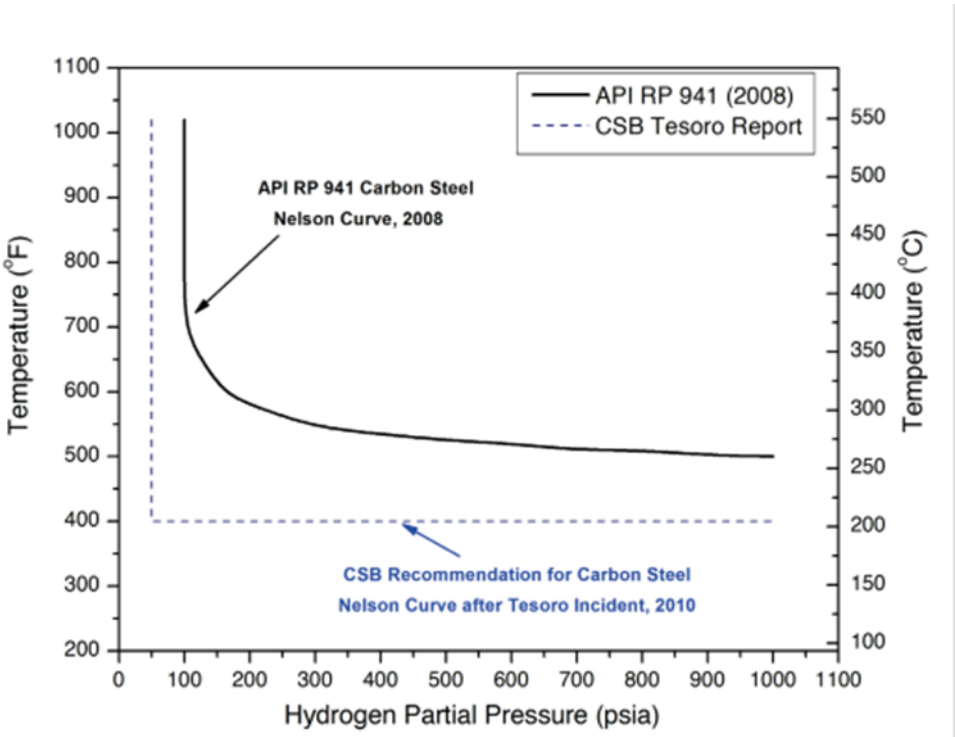

Figure 11. CBS recommended limited values for temperature and hydrogen partial pressure for carbon steel.

2.6 API 941 content and usage

This is a Recommended Practice on “Steels for Hydrogen Service at Elevated Temperature and Pressure in Petroleum Refineries and Petrochemical Plants”. It was initially released in 1970, and since then, various updates have been made. API standards are published to inform manufacturers, suppliers, and employees about the proper selection of materials, their characteristics, and preferable conditions of usage, as well as inspection methods and safety measures for the prevention of equipment damage. It contains the Nelson Curves diagram, HTHA information on carbon steel and carbon steel alloys (0.5Mo Steel, 1.25Cr-0.5Mo Steel, 2.25Cr-1Mo steel), and their operating limits. It also includes a thorough description of the HTHA phenomenon, the failure mechanism's stages, and prevention and inspection methods for HTHA [6].

There is also a discussion of the suitability of those methods. It is concluded that no optimal method can detect HTHA on its own. Ultrasonic techniques are the most likely to find HTHA, but only after fissures have been created [9].

The major adjustment to the Nelson curves came from more recent accidents, such as the Tesoro incident, where studies determined that HTHA caused equipment failure in carbon steel operating below the Nelson curve. The equipment had not been heat-treated after welding, and all the damage found was in the heat-affected zone near a weld [23]. Therefore, the latest API RP 941 (8th edition, 2016) proposes weld sections as the most likely places for HTHA and contains in the Nelson diagram a curve indicating the safe operating limits for the non-PWHT (Post Weld Heat Treated) carbon steel.

Because of the API 941 modifications, the initial metallurgy option may no longer be suitable. Plants may consider doing an engineering evaluation on equipment and pipes running under the circumstances covered by the most recent Nelson curves to ensure that the material is appropriate for continuing operation.

Based on this risk, equipment should be examined following risk management plans. These plans are targeted at reducing items of equipment considered susceptible by risk assessment [9]. The suggested actions are:

1. Increased examination during outages could include destructive testing when equipment is retired or removing a sample from the equipment.

2. Replacement of old equipment with more resistant alloys.

3. Lowering of the operating conditions, particularly temperature, because they influence HTHA.

4. Establishment of an Integrity Operating Window (IOW), that is clearly understood throughout operations, including what to do if there are any deviations. IOWs are limits specifying the variables may influence material credibility [24].

Other segments of the API manual, apart from the 941, can be consulted for better equipment evaluation. For example, the API RP 581, Risk-Based Inspection Technology, is a recommended practice for quantitative risk-based inspection developed and published by API (RBI). The second edition, released in 2008, sought to quantify risk variables [2] . As a result, P_v was introduced, a parameter that was a function of the hydrogen partial pressure (P_{H_2}), temperature, and time. This parameter has been utilized to group and graph destructive versus non-destructive test findings based on the degree of HTHA exposure. This P_v option has subsequently been removed from API 581 3rd Edition 2016's newest version. The equation for the P_v parameter is [25] :

$$P_v = logP_{H_2} + 3.09 \times 10^{-4}\, T(\log t + 14)$$

In this equation T is the operating temperature, t is the time in service and P_{H_2} is the hydrogen partial pressure.

The 2016 modification takes a more cautious approach, particularly for carbon steels and C-0.5Mo steels, for which the latest version of API 581 assigns high susceptibility to equipment operating at temperatures above 177°C and hydrogen partial pressures exceeding 0.345Mpa. These parameters are considered relatively conservative in the PWHT and non-PWHT carbon steel curves in the AP 941 [9].

2.6.1 Inspection methods

High-Temperature Hydrogen Attack is challenging to detect. Macroscopic investigation, through naked eye, is impossible since apparent, to the eye cracks, mean that the equipment has failed, and the failure is irreversible in any way. The damage may be microscopic, localized, and occurs in small parts of the equipment. During the incubation period, in the early stages of the attack, voids, that don't exceed the size of a nucleus and micro-fissures are difficult to detect. The detection is easier during the advanced stages of the attack, using NDE (Non-Destructive Evaluation) techniques. However, where the final failure of the equipment is much more likely to happen. HTHA can occur on welds, weld HAZs, or the base metal. Welded regions make it more challenging in detection, due to signal interruption. The variation between the degrees of damage in these areas demands a thorough inspection of all these areas. Depending on the region of HTHA evaluation different techniques should be used.

The method preferred to detect HTHA is the special non-destructive testing (NDT) technique. The examination of HTHA for the base metal is through ultrasonic testing. The most effective method for examining the base metal that detects fissures is using a frequency-dependent backscatter with a velocity ratio and spectral analysis techniques [15].

The backscatter can detect and measure the depth of the attack, and the velocity ratio and spectrum analysis are used to confirm the backscatter findings. The methods used for HTHA detection on the weld are high-frequency shear wave or angle beam spectrum analysis techniques. They can detect the damage during the saturation stage. Other methods can detect HTHA only when there is significant damage. Some researchers reported satisfactory results using different methods. According to Nugent et al. [9], phased-array UT (PAUT) and Time of Flight Diffraction (TOFD), with or without the total focusing technique (TFM), yield the best outcomes when analyzing HTHA. They offered step-by-step instructions on how to use these techniques for accurately diagnosing and assessing HTHA damage. Additionally, Neve et al. also indicated that PAUT, TOFD, and TFM produced better results than AUBT.

The reliability of the method used is subjective. The trustworthiness of the results depends on various factors, such as the selection of the correct technique, the right selection of needed parameters and the skill of the specialist who executes.

2.6.1.1 Advanced Ultrasonic Backscattering Technique (AUBT)

AUBT is first employed as a screening method to detect microcracking in parent material, which is quickly recognized by scanning with a linear beam transducer. AUBT is a rapid screening technique that covers large surfaces while searching for HTHA indications [26],[27]. Based on the magnitude of reflections induced by micro-cracking, the approach allows for the early detection of possible HTHA sites and measuring of the depth of the attack. It is used to predict the remaining life of the equipment as well as its fitness for service. The results appear in the form of different patterns. It helps differentiate HTHA from other inclusions or impurities [25] . Locations are then selected for further HTHA assessment using the velocity Ratio or Spectrum Analysis. The initial scan of the target region is performed in this procedure using a 5MHz L-wave probe. The patterns are distributed below.

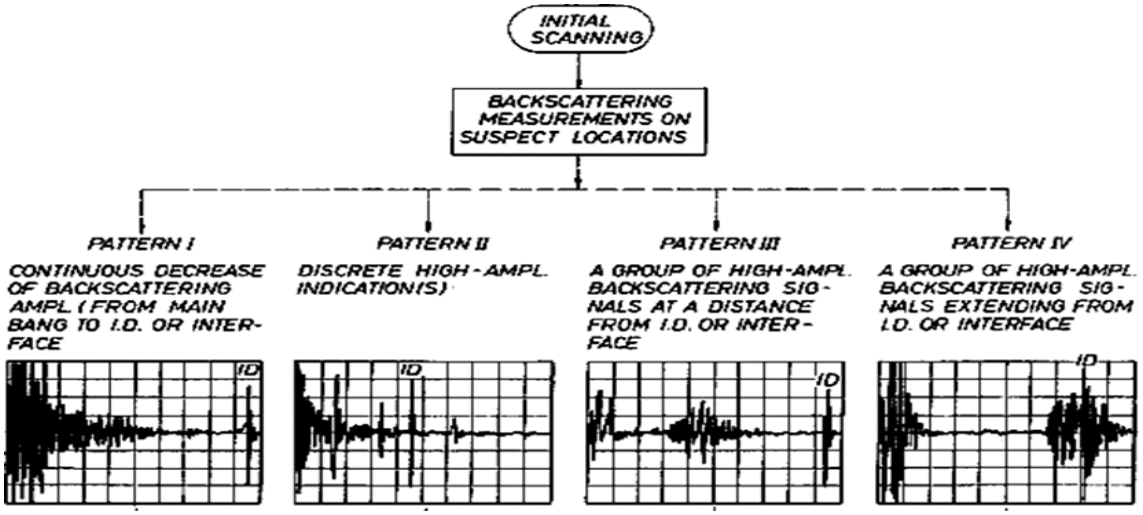

Figure 12. Patterns of AUBT indicating the type of damage.

- Pattern l indicates the internal thickness flaws of the specimen.
- Pattern II presents the linear and horizontal defects parallel to the internal equipment surface.
- Pattern III shows the internal damage caused by the advanced HTHA mechanism.
- Pattern IV presents the internal damage caused by initial or advanced HTHA mechanisms.

Different techniques follow this method according to the pattern that appears during the AUBT inspection. For example, if Patterns I and IV appear, the method is followed by a velocity ratio measurement and a Spectrum Analysis. In the case of patterns II and III, the technique is followed by a velocity ratio measurement, Spectrum analysis, and frequency dependency of the scattered wave.

2.6.1.2 Velocity Ratio

The Velocity Ratio technique uses the difference between longitudinal and transverse sound velocities in healthy material versus material attacked by HTHA. Both longitudinal and transverse sound velocities can shift in an area of material impacted by HTHA, but not to the same extent. The ratio of longitudinal to transverse sound velocities increases in the affected area. It also means that the computed velocity ratio will increase throughout the total thickness, which includes both impacted and non-affected material [26] . It can differentiate between inclusions formed during the material's manufacture and the methane-filled ones due to HTHA. Simple digital UT equipment with a 5MHz straight beam probe, for example. It is a simple and inexpensive method that does not require much-specialized equipment but cannot be utilized on its own. This method only detects HTHA when the affected thickness is larger than 15% of the specimen thickness.

2.6.1.3 Power Spectrum Analysis

Power Spectrum Analysis is a technique that detects HTHA throughout the whole material wall thickness, by measuring the HTHA index from the Power Spectrum of the backscattering signal [19] . It can discriminate between the inclusions formed during equipment manufacture and those filled with methane created by HTHA at grain boundaries. An HTHA Index is calculated using the Power Spectrum of the backscattering signal at the center frequency of the wave generated and compared to a non-affected reference to detect HTHA. The power spectrum allows the backscattered energy of material abnormalities to be quantified. It is tiny at the start of the process and grows as micro cracks emerge and the size of the anomaly increases. The following formula is used to determine the HTHA Index, which is equal to a structure variation:

$$HTHA\_index = log\ (PSM/PSR)$$

Where PSM = Power Spectrum of Material that is affected by HTHA and PSR = Power Spectrum of Reference the material that is not affected by HTHA.

2.6.1.4 Time of Flight Diffraction (TOFD)

For the inspection of the HAZ area or weld section, a TOFD method (Time of Flight Diffraction) can be used in combination with an angle beam shear wave technique, like the Phased Array technique [25] . Velocity ratio and spectrum analyses can be used after to confirm the results of TOFD [26] . TOFD uses diffraction wave characterization instead of an echo reflection, making it highly possible to detect the appearance, the location, and the size of cracks. TOFD, besides the HAZ side inspection, can be used on the base metal. For this method, a 6MHz TOFD probe is needed. Spectrum Analysis is required to differentiate micro-cracks and other weld defects discovered through this technique. It is a highly reliable technique and can detect HTHA attack at early stages, differentiating successfully HTHA from failures caused by other mechanisms. It is a non-intrusive technique making monitoring possible up to 400 °C.

2.6.1.5 Wet Fluorescent Magnetic Testing

If the internal surface is accessible, surface cracks can be detected through Wet Fluorescent Magnetic Particle Testing (WFMT). During this method tiny particles are spread over the surface of a specimen, which is being magnetized. These particles accumulate on discontinuities like cracks, inclusions, seams, etc. Due to their high magnetic permeability, they are drawn to small magnetic leakage fields that are created at discontinuities. An experienced technician is needed to construe the signs given during the inspection.

Magnetic Testing can also be conducted using dry as powder particles. However wet particles, as a solution in water or petroleum-based medium, is preferable. In this method the particles are smaller in size, and the liquid medium makes it easier for them to move and accumulate in tiny leaks. WFMT is thought to be the most efficient method for detection of tiny defects. In the regard of inspecting of large components high currents are necessary. Also, for the examination of both longitudinal and peripheral dimensions tests should be performed in both directions. Only degreasing of the material and insignificant cleaning are required for the inspection [28].

2.6.2 Prevention methods

Since HAZ sections are more susceptible to HTHA due to the existing stresses, a method to reduce the material's sensitivity should take place.

2.6.2.1 Post-Weld Heat Treatment (PWHT)

Post Weld Heat Treatment is used to reduce internal stresses created during the welding process. It is a controlled reheating process of the metal. The reheating of the material also stabilizes alloy carbides [8] , reducing the amount of free carbon and improving, thus, the hydrogen attack resistance of the material [15]. Reheating is conducted at a lower temperature than the critical transformation one. The most well-known and widely used methods are Stress-Relieving [3] and Post- Heating. Post-Heating is done to reduce the risk of Hydrogen Induced Cracking, that appears after welding up to 7 days later. Post heating allows hydrogen to diffuse to the exterior of the material, especially in the welded and HAZ regions where hydrogen may be trapped due to rapid cooling after the weld procedure. The weld should not cool below 93.3°C. The region under post-heating treatment must be maintained for a specified time frame, depending on the material and the thickness, under specified temperature. Thus, the probability of cold cracking is reduced, when the part reaches room temperature, through the diffusion of hydrogen out of the material. The stress-relieving procedure involves the heating of the weld area at a specific temperature, higher than that of post-Heating, and a longer amount of time. The temperature region, for most carbon steels, is between 480°-750° C, depending on the material [29]. The temperature must not allow phase transformation. The weld region is covered by a resistance heater, electrically and thermally self-insulated. Temperature increase reduces the material's yield stress and allows the diminution of residual stresses due to plastic flow. For better quality treatment and to prevent unwanted changes in shape, the equipment should be treated on the bed of the welding procedure.

The benefits of PWHT are these [9]:

- Reduces the existence of residual welding stresses.

- Improves the material's ductility.
- Reduces the risk of brittle fracture (due to increased ductility).
- Reduces the diffusible hydrogen (prevention of hydrogen damage mechanisms).

PWHT increases the material's price and the duration of its fabrication. Thus, some manufacturers skip it.

2.6.2.2 Acoustic Emission Testing (AET)

Acoustic Emission Testing involves attaching small sensors to a component that is being tested. The sensors transform the stress waves into electrical signals, which are then transferred to a processing computer. The waves are collected when the component is exposed to external stimuli, such as high pressures, loads, or temperatures. There is a more significant release of energy as the component's damage increases. The activity and intensity of the acoustic emission are monitored and used for measuring structural integrity and component health monitoring [7].

Acoustic emission is like vibrations released due to stress, like an earthquake. Unlike destructive testing, this technology continuously monitors a component for faults, allowing massive structures and machinery to be monitored while in operation with minimal disruption. Acoustic emission sources and thus damage can be located utilizing several sensors. Signal analysis can also determine the presence of various source processes. This technique has been used during the equipment's cool down.

Compared to other approaches, acoustic emission offers numerous advantages. Among them are:

1. The ability to detect a variety of damage mechanisms early on, such as fiber breakages, friction, impacts, cracking, delamination, and corrosion.
2. It can be done in the field, during the proof or development testing.
3. Can find damage sources and distinguish them using audio characteristics.
4. Evaluates the building or machine in actual conditions.
5. Operable in hazardous situations such as high temperatures, high pressures, and corrosive and radioactive conditions.

6. Can detect damages in problems that are difficult to access with traditional non-destructive testing techniques.

However, there are certain drawbacks to the method:

1. First, this method is limited in evaluating material integrity. Further, an inspection is needed to assess the problem entirely. It cannot produce information about the vicinity of the crack or about any of its characteristics.

2. It cannot detect problems that may exist but do not move or grow.

3. It may be slower than other non-destructive testing methods.

2.6.2.3 Cladding

HTHA-resistant linings or coatings that either function as insulators to lower metal temperature or as well as reducers of hydrogen permeation. Utilizing HTHA resistant coating, reduces the amount of hydrogen that diffuses into the metal. According to Archakov and Grebeshkova [9], the hydrogen absorption of widely used industrial materials rises from aluminum, which has the lowest rate, to carbon steel, which has the highest. They propose mathematical formulas, in accordance with Fick's Laws, to determine the hydrogen pressure in between the neighboring metals. The Nelson curves can be used to support the evaluation of HTHA safety once the pressure and temperature at the liner and metal interface are known. Austenitic claddings are thought to be the most effective due to smaller, by an order of magnitude, hydrogen diffusivity and high resistance to corrosion [15].

2.6.3 Destructive Evaluation

The most effective method for HTHA evaluation is the destructive one, by cutting a piece of equipment for metallographic evaluation. Unfortunately, it is highly likely that the equipment will be rendered unfit for service. Metallographic examination is conducted by the preparation and polishing of samples from different regions of interest from the equipment (Base metal, HAZ, weld metal) and then microstructural examination using an optical microscope. For more detail a Scanning Electron Microscope (SEM) or a Transmission Electron Microscope (TEM) are used. Breaking the sample is also useful for the evaluation of the crack surface, using the SEM microscope. Due to the development of many methane blisters, the HTHA affected regions may show areas of dimpled intergranular fracture.

Mechanical properties can also be evaluated to discover HTHA. Tensile testing, hardness testing, impact testing, and fracture tip opening displacement are all examples of mechanical testing. SEM analysis is frequently used in conjunction with these tests to add on the appearance and location of bubbles or cavities. A quantitative indicator of HTHA damage is the percentage of the shift in mechanical property. The loss of reduction-in-area during a tension test at room temperature, according to Shewmon [9], is "the most obvious evidence of hydrogen attack". Alternations of mechanical characteristics may depend on the interaction between several forms of microstructural damage. For example, considerable decarburization may cause a reduction in strength and an increase in elongation because of softening, whereas grain boundary fissuring may cause a reduction in both elongation and strength. The existence or saturation of atomic hydrogen may result in an increase in hardness in the affected areas.

2.7 Prior cases of HTHA and conclusions

2.7.1 Tesoro Anacortes Refinery

A tragic accident also caused by the HTHA failure of a heat exchanger occurred in the Tesoro Anacortes petroleum refinery. The NHT (Naphtha Hydro-Treater) unit removes sulfur, nitrogen, and oxygen contaminants by heating naphtha to above 315 °C and combining it with hydrogen at pressures greater than 4,14 MPa. The initial portion of this procedure requires the use of six heat exchangers. The failure appeared on the E-6600E and E-6600B heat exchangers, which was attacked and bared a long crack. The equipment was fabricated from carbon steel with a very low concentration of Cr and Mo (C 0.27 %wt., Cr 0.12%wt., Mo 0.025%wt.). The material was not Post Weld Heat Treated. The regions adjacent to welds, high stressed areas were attacked. More specifically, the damage was observed in the heat-affected zones and the fusion boundaries of the welds. The crack formed along the HAZ coarse grain boundaries [22].

The equipment was operating below the limits set by the Nelson Curves. Before the accident, corrosion reviews were conducted, for example damage mechanism hazard reviews, but HTHA damage was not detected. It is possible because these reviews relied on the operating conditions defined by design and not the actual ones. As a result, the portion of the equipment operating beyond the limits, the hottest equipment section, was not considered.

During the start-up of the exchanger, hydrocarbon leaks and fires were common and additional personnel attended to them. However, management did not investigate such incidents' appearance further and normalized their occurrence. Two leaks appeared a little while before the incident, during startup, but were not taken under serious consideration. Tesoro expected them to cease once operating temperatures were reached. During, the startup of the specific group of heat exchangers it was usual to wait for them to subside as it happened when the equipment reached the typical operating temperature. Immediately

before the rupture, there was an increase of 75°C. After approximately three minutes, the explosion released an amount of naphtha and hydrogen that auto- ignited, creating a fireball [23] .

The mechanical properties of the equipment were severely lacking because of the HTHA cracking damage. The additional stress from the start-up of the remaining heat exchangers was sufficient to cause critical mechanical strength deterioration. Long and deep cracks were detected in the B heat exchanger, which was not affected by the explosion. Both exchangers were deeply affected by the HTHA mechanism.

2.7.2 Kashima Oil Refinery

Prior to the Tesoro Anacortes accident, there was another explosion that proved deadly in 1982. The explosion occurred in Japan's Kashima Oil Refinery [9]. A Carbon-Steel pipe of the desulphurization unit failed. During the metallographic evaluation of the failed pipe, HTHA damage was detected in the material's interior. Many small cracks appeared along with decarburization evidence. The operating temperature of the equipment was below 200°C. Furthermore, there was no thickness diminution, so the failure was attributed to highly brittle conditions.

2.7.3 Kuwait National Petroleum Company

Another HTHA mechanism damage occurred in the Kuwait National Petroleum Company. The KNPC owned a reactor made of 2,25Cr–1 Mo steel [16]. After four years of operation, the reactor's inner wall, in the HAZ side, developed cracks. Grinding was used to eliminate the cracks, and the connection was re-welded. However, after six years, more cracks in the HAZ reappeared in various parts of the vessel. The restoration took a long time and was costly, yet it did not eliminate the problem. Instead, the vessel's internal pressure was required to be reduced from 19.3 MPa, which was the specified by design operating pressure, to 8.96 MPa, and the cracks to be carefully observed. This was a temporary solution as it also reduced the reactor’s production capacity. The handling of this situation proves that there is limited expertise concerning this mechanism and ways to cope with it.

3. HTHA in a heat exchanger of an oil refinery

The Aspropyrgos Refinery of the Hellenic Petroleum Group (HELPE) faced the failure of a heat exchanger in 2014. Leakage appeared on the outer surface of the heat exchanger M-9210 while a cleaning process of the exchanger tube was being held. Steam leaked out of a crack of about 0.5m long near the welded area, the L3 part of Figure 13 drawing below

(Figure 13). They assigned the Laboratory of Materials of the University of Thessaly the investigation of the causes of this incident.

The Aspropyrgos Refinery was bought from the Greek Government in 1975. As a petroleum refinery it was inaugurated in 1958. It is in the periphery of Athens in the Aspropyrgos industrial area. The plant processes atmospheric residues and vacuum gas from the Aspropyrgos and Thessaloniki refineries to produce higher value products. Upgrading of the hydrotreating and naphtha reforming units with the operation of the TAME unit took place in 2004. The heat exchanger under evaluation is part of the naphtha creation unit and was manufactured in 2006.

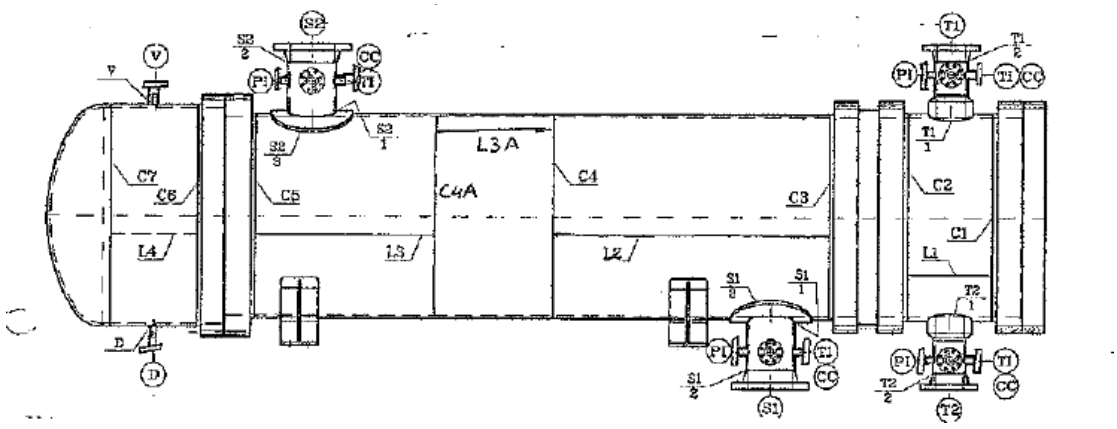

Figure 13. Drawing of the M-9210 exchanger.

The material of the heat exchanger from the Aspropyrgos refinery was carbon-steel (SA 516M Gr.70). According to the material certificate, the carbon (C) content was 0.15 (%wt.). It was an hypoeutectoid carbon steel tube that operated at 310°C and 2.9 MPa. The operating temperature and hydrogen partial pressure exceeded the limits for carbon-steel (welded and non PWHT) and carbon steel (welded and PWHT) designated by the Nelson curves. The chances of the failure being contributed to HTHA are very high. There may also be a synergy of other mechanisms related to HTHA, but they contributed to the initiation of the crack and not the final failure [1].

Operational Temperature	310 °C
Operational Pressure	29 bar + FV
Material	SA 516M Gr. 70
Content	H2 - 8 bara after 07/2014 H2 - 14 bara prior to 07/2014 S contents - 400 ppm after 07/2014 S contents - 1000 ppm prior to 07/2014 Hydrocarbons

Table 1. Operational characteristics of heat exchange M-9210.

The heat exchanger during manufacturing underwent a welding process GMAW and SAW, in 2005. This fusion-welding process is widely used for the fabrication of pressure vessels used for storage or processing of petrochemicals [16]. The weld was a double V-shaped one, with an angle of 60 degrees. The thickness of the tube, 20mm, created the need for three beds. Due to uneven heating, subsequent cooling, and uneven distribution of non-elastic strains, residual stresses possibly formed during welding. Heating causes the metal to expand in a non-uniform manner, which can result in yield. In addition, the metal undergoes non-uniform contraction during cooling, which could contribute to increased yielding. Non-elastic strains arise from these heating and cooling cycles, resulting in residual stresses. These strains can cause cracking immediately after welding and sometimes throughout the equipment's service life. Hydrogen trapped in the HAZ regions of the weld due to rapid cooling may cause cold cracking of the material. Stress build-up, fatigue failure, and fracture can all be caused by tensile residual stresses around the weld area and the HAZ. Also, the material of the filler is different from the base metal, usually poorer in carbon. Thus, different microstructures possibly develop.

Post weld heat treatment did not take place after the welding procedure. Thus, the HAZ section remained susceptible due to stress existence.

The phase diagram, of the phases of carbon steel, reveals the expected phases of a 0.15 (%wt.) carbon steel during the welding procedure.

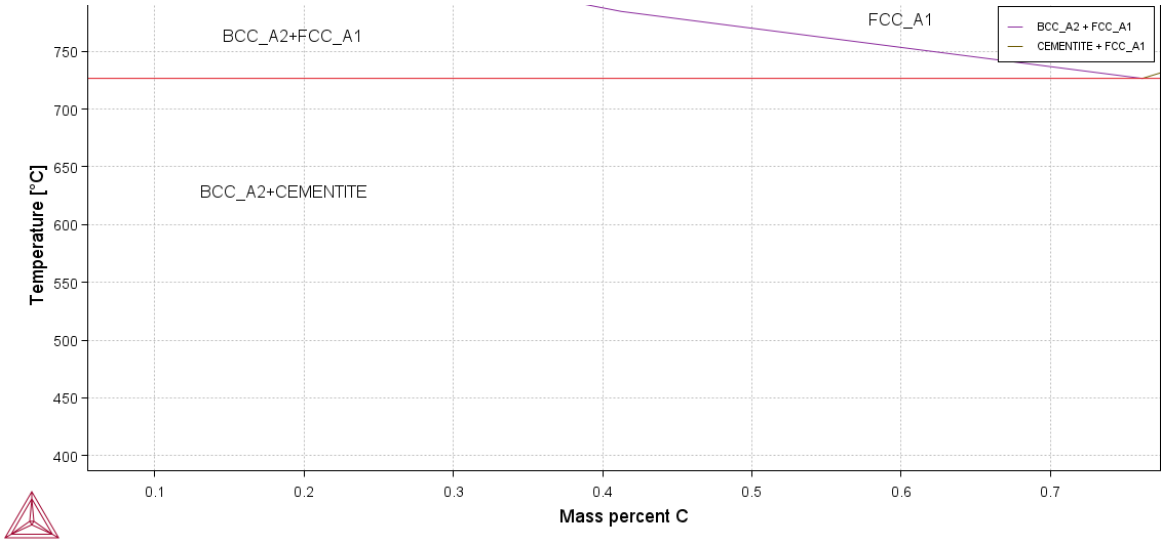

Figure 14. Phase diagram for carbon steel, using Thermocalc for temperature up to 750°C.

According to the diagram, for a composition of 0.15% wt. of C, ferrite and cementite appear, and there will be a ferrite-pearlite matrix. The pearlite will contain cementite carbides, and ferrite will be the continuous phase.

4. Methodology-Experimental Procedures

4.1 Macroscopic examination

A segment cut from the exchanger outer tube was firstly examined with the Stereoscope to gain better insight on the crack propagation direction. The specimen taken for sampling was cut from the site of the weld L3, where the main crack is located. The specimen contained part of the main crack that demonstrated failure.

Figure 15. Piece of the external tube of the heat exchanger M-9210.

The main crack is shown up close, in the two pictures below (Figure 16), (Figure 17). The bottom half of the main crack corresponds to the first image, and the top half, corresponds to the second.

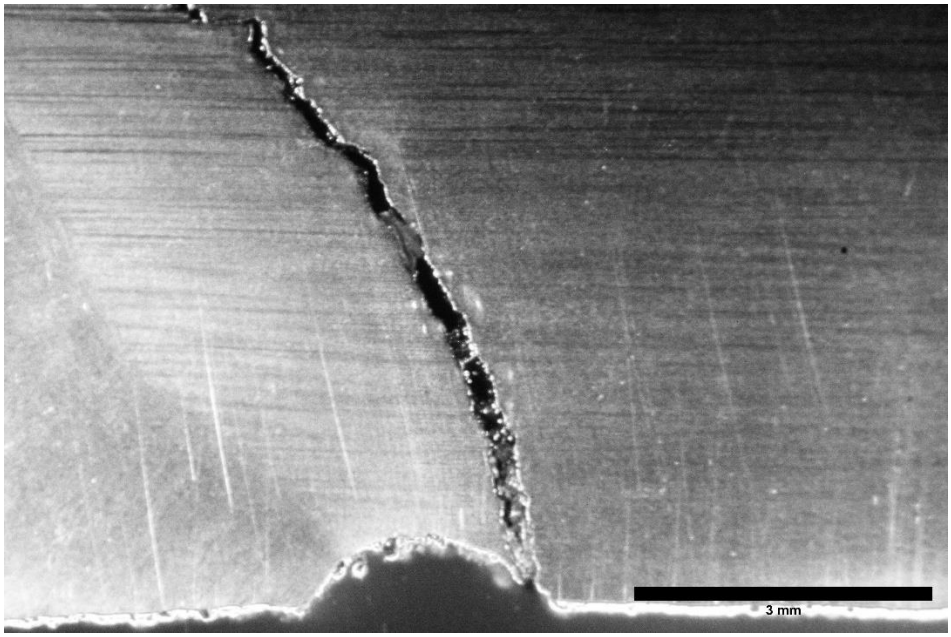

Figure 16. Bottom half of the main crack, using a stereoscope

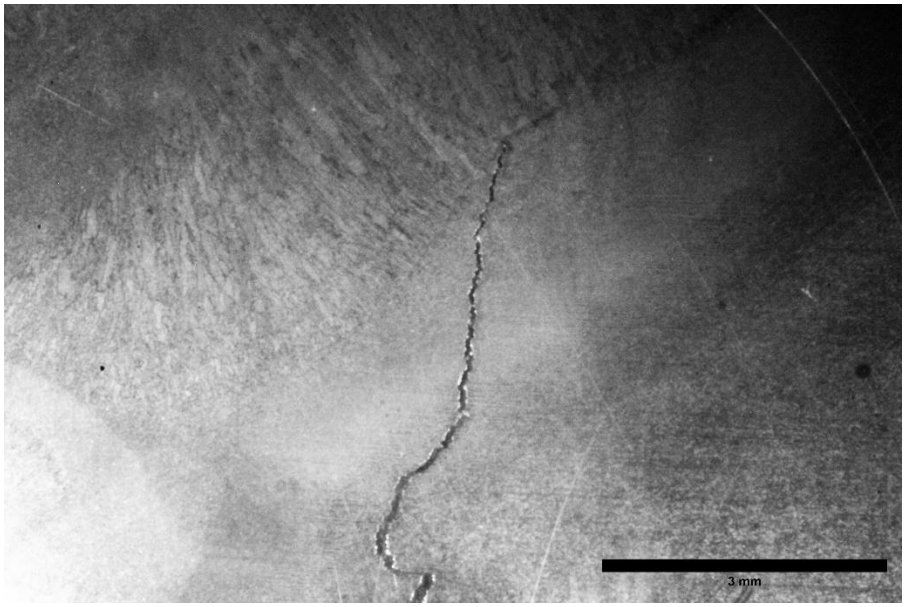

Figure 17. Top half of the crack, using a stereoscope

4.2 Metallography

The piece cut, from the exchanger, is prepared for optical examination, with a microscope, to investigate the failure mechanism that took place.

4.2.1 Metallographic Analysis Preparation

Metallographic analysis was performed on the specimen shown in the picture below (**Error! Reference source not found.**). The areas examined were the portion around the main crack and some sections away from it. Firstly, the process for metallographic preparation involved cutting a specimen from the tube with Struers and mounting it in resin. Then grinding, with silicon carbide abrasive papers (SiC) 120, 180, 220, 320, 500, 800, 1000, 1200 grit and polishing with a diamond paste of 1μm on a short-nap cloth, was performed. For achieving better surface quality and minimization of temperature increase during grinding water was sufficiently provided and for polishing a kerosene lubricant. Lastly, the specimen underwent chemical etching with Nital 2% followed. The Nital 2% composition is 2mL HNO_3 and 98 mL ethanol.

4.2.2 Optical Microscopy

The optical examination of the specimen was through an Optical Metallographic Microscope, the Leitz «Aristomet», at magnifications varying from 50X-1000X.

4.2.3 Fractographic examination

Fractography was carried out using a SEM JEOL JSM-5310. The specimen was cracked open and cleaned from deposits, in order to examine the main crack surface. However, some deposits remained on the surface, but didn't prevent surface examination.

4.3 Hardness measurement

Moreover, a hardness measurement took place. Microhardness measurements were conducted on selected specimen areas, specifically on the base metal and the heat-affected zone. For the measurement, a WOLPERT 402MVD micro-hardness tester with a digital auto-tuner. A load of 300 gr on a Vickers scale was implemented.

5. Results and Discussion

5.1 Macroscopic examination results

The examination of the piece, by stereoscope, reveals that the main crack propagates in the direction of the axis of the tube. It starts at the internal surface of the equipment. The

direction of the crack is parallel to the axis direction but shows abrupt change of direction, vertically to the axis direction, as indicated by the red arrows (Figure 18). The change in direction is limited to a small part of the crack, in the conjunction of the double V weld. The crack as it propagates, closing into the outer tube surface, enters the HAZ section of the weld and continues parallel propagation to the tube axis dimension.

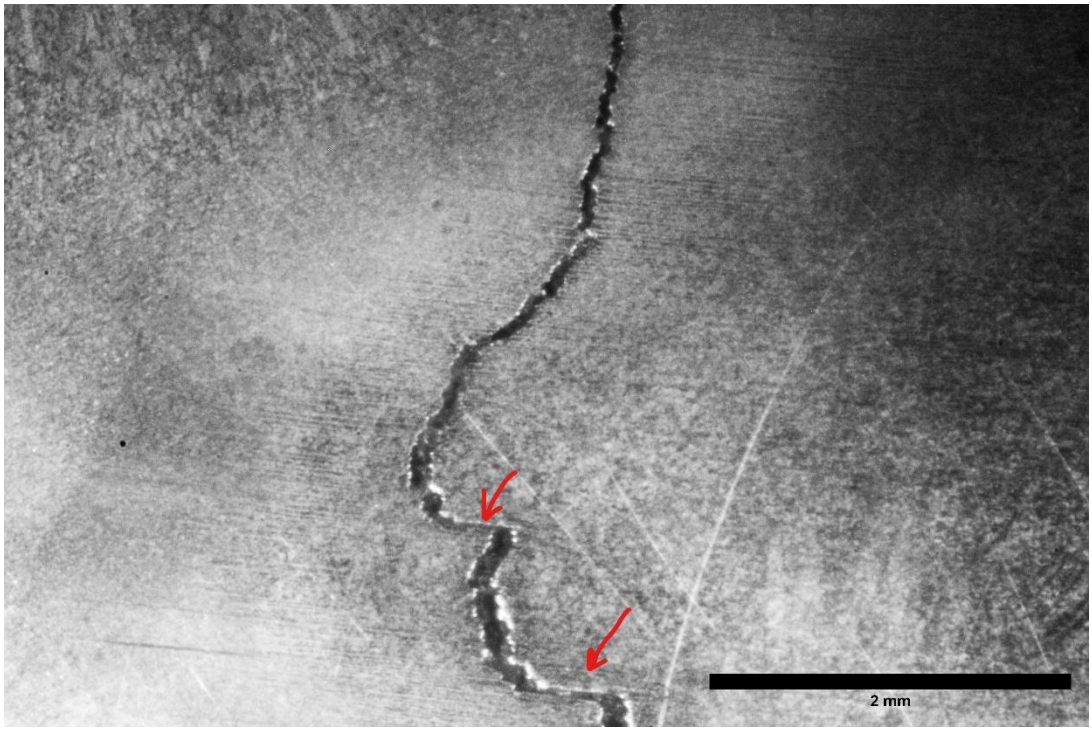

Figure 18. Abrupt change of direction of the crack, vertical to the tube axis direction.

5.2 Microstructural description of base metal and HAZ of weld

5.1.1 Chemical Analysis

The results of the chemical analysis (%wt.) are given below.

	C	Si	Mn	S	P	Cr	Ni	Mo	Al	Cu	N
M-9210	0.12	0.25	0.98	0.01	0.01	0.04	0.08	0.02	0.03	0.29	0.004
Certificate No.703284A	0.15	0.29	1.1	0.005	0.008	0.05	0.09	0.001	0.034	0.35	0.007
SA 516M Gr. 70	0.28 max	0.13-0.45	0.79-1.3	0.035 max	0.035 max	-	-	-	-	-	-

Table 2. Chemical Composition

The chemical analysis indicates low carbon-containing steel, hypoeutectoid carbon-steel. The chemical analysis reveals that the material is indeed within the specifications of the reported grade in the material certificate.

5.1.2 Microstructure of the BM and HAZ of the weld

The examination of the specimen through the microscope reveals a ferritic and pearlitic matrix. The white portion is the ferrite, and the darker color is the pearlite (Figure 19).

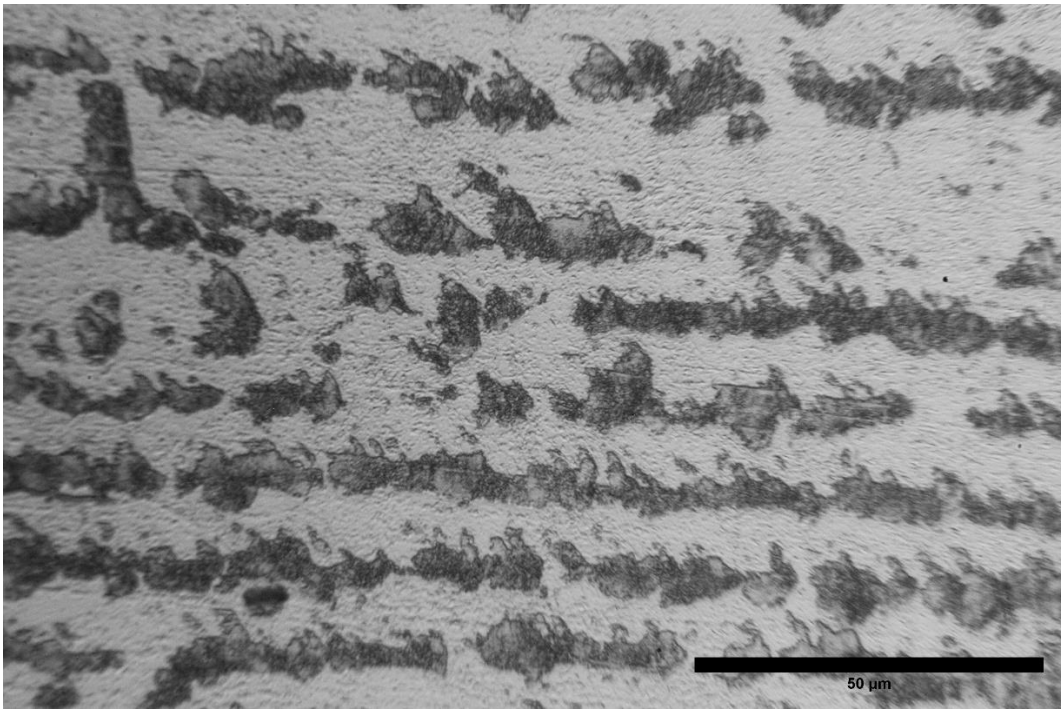

Figure 19. Ferritic and pearlitic microstructure of the material in the base metal.

On the base, metal ferrite is the main phase we encounter. Pearlite content is lower than ferrite but significant non the less since pearlite has a higher carbon composition, due to the cementite carbides in the matrix. Banding, vertically to the main crack direction, is observed between the pearlitic and ferritic matrixes of the BM. Banding between the ferrite and the pearlite facilitates fissuring, providing an easy path for crack growth as a weak interface, and initiating micro-fissuring perpendicular to the main crack direction [30] . Banding is a result of cold work during the fabrication of the equipment. The specimen was slightly over etched for the different phases to be more accentuated (Figure 20Figure 20).

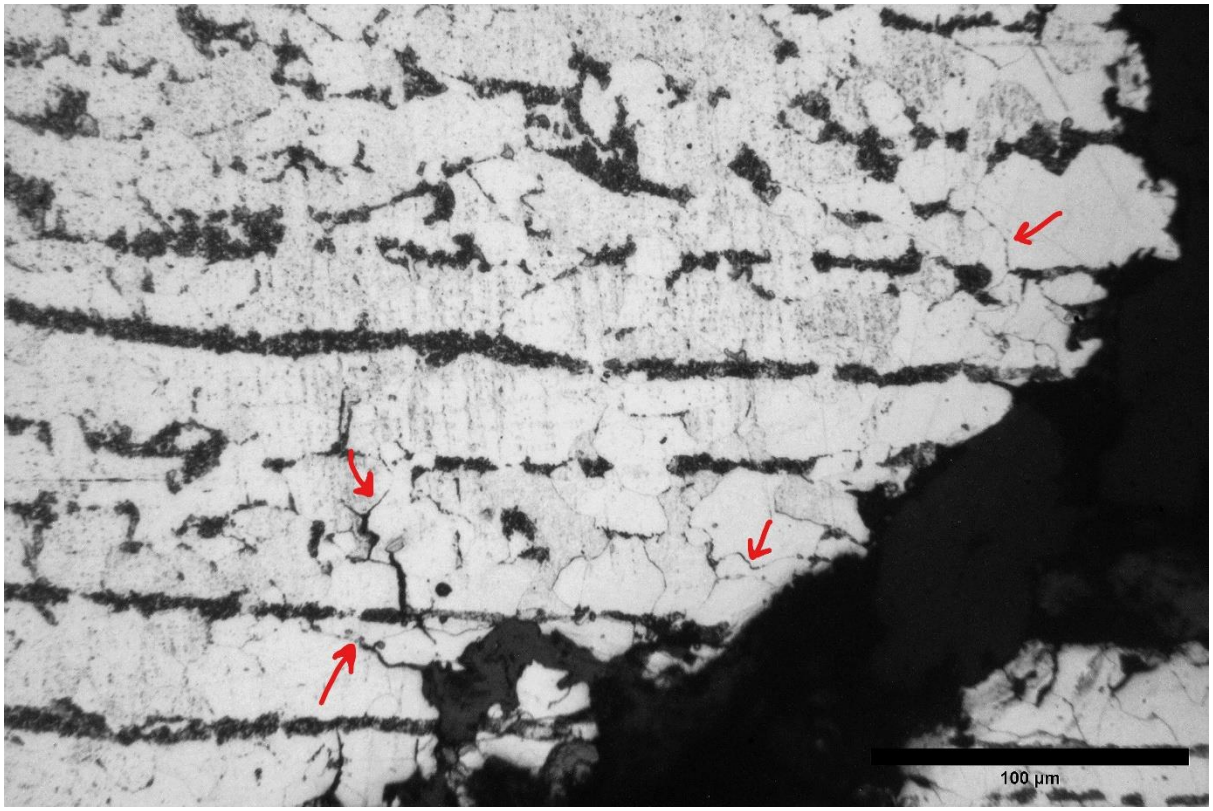

Figure 20. Intergranular cracking of the grain boundaries and banding in the base metal.

The crack tip advances in the HAZ of the weld. The microstructure of this region is different from the base metal. Spheroidization of the pearlite is observed, dissolution of the banding. Also, Widmanstätten ferrite is detected (Figure 21).

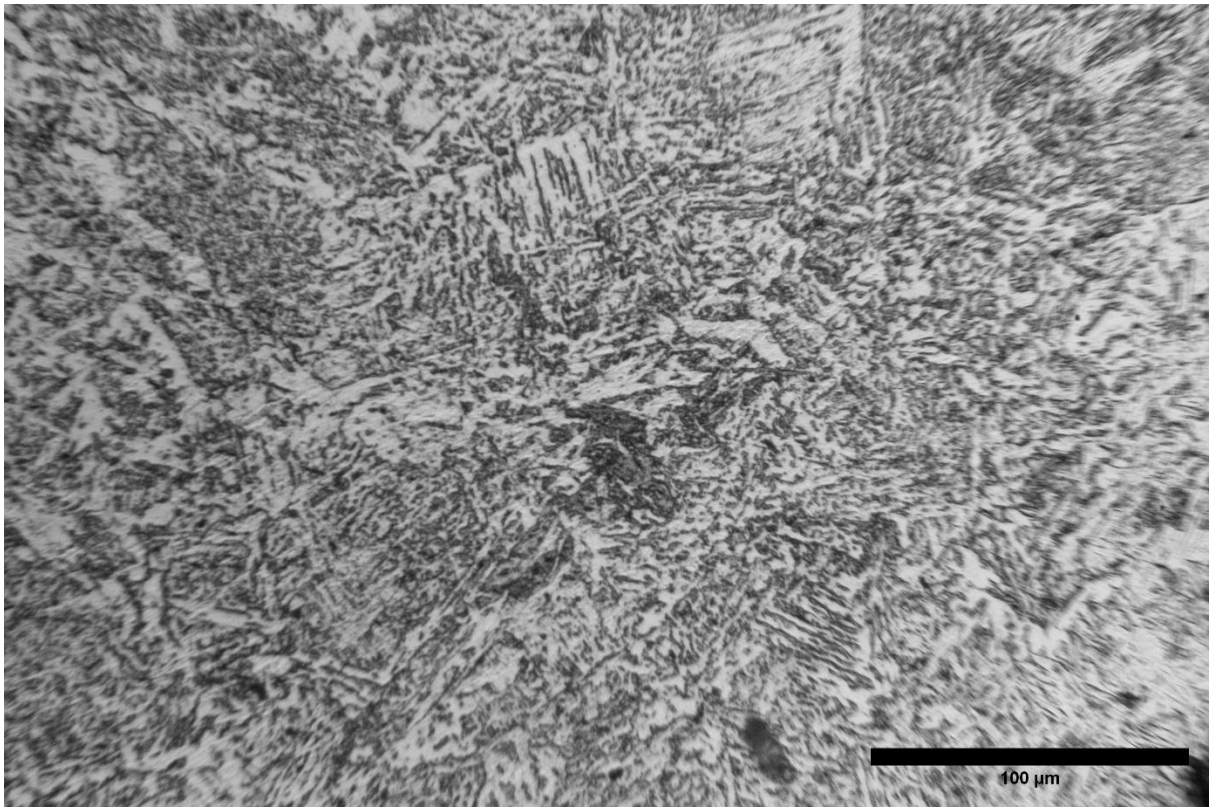

Figure 21. HAZ side microstructure. Pearlite spheroidization and Widmanstätten ferrite.

5.2 Crack initiation and crack path – microstructural aspects

The length of the main crack reaches 0.5m. The main crack was observed on the boundaries of the HAZ and the BM zones of the welded metal. It follows a path close to the weld and advances within the thickness. It initiates on the base metal at the internal surface. The top half of the crack advances into the weld's HAZ side. Hydrogen gains access through the crack to the metal's interior. The advance of the main crack is facilitated due to further surface and internal decarburization. The main crack is intergranular and seems to propagate by the coalescence of elongated voids and fissures. Numerous intergranular micro-cracks are observed on grain boundaries (Figure 22). The damage is severe. In some areas the optical microscopy examination reveals elongated voids, which consume almost entire pearlite grains. In some areas there is significant branching of fissures, especially near the main crack. On the banks of the main crack there is evidence of brittle grain detachment.

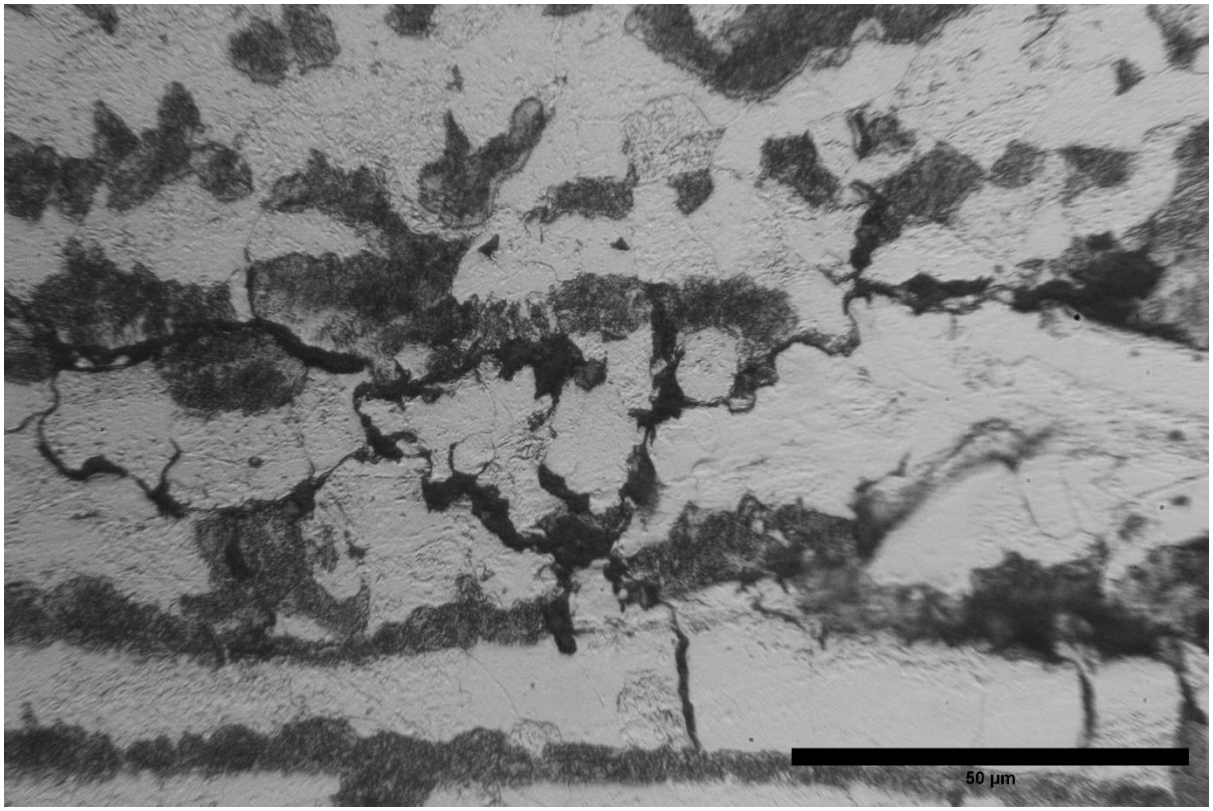

Figure 22.Intergranular propagation of fissures and pearlite grain consumption.

The main crack abruptly changes direction in the middle portion. The cause may be the intense stress created by the weld. The change of direction appears almost at the conjecture of the double V weld. In the sections where the main crack changes direction intense cracking appears, perpendicular to the crack propagation direction.

Banding facilitates the propagation of fissures. The fissures travel along the grain boundaries of the pearlite colonies and occasionally cross vertically, through the ferrite matrix. These paths seem to be created for the fissures to propagate to the neighboring pearlite colonies, probably in search of a carbon source (Figure 23).

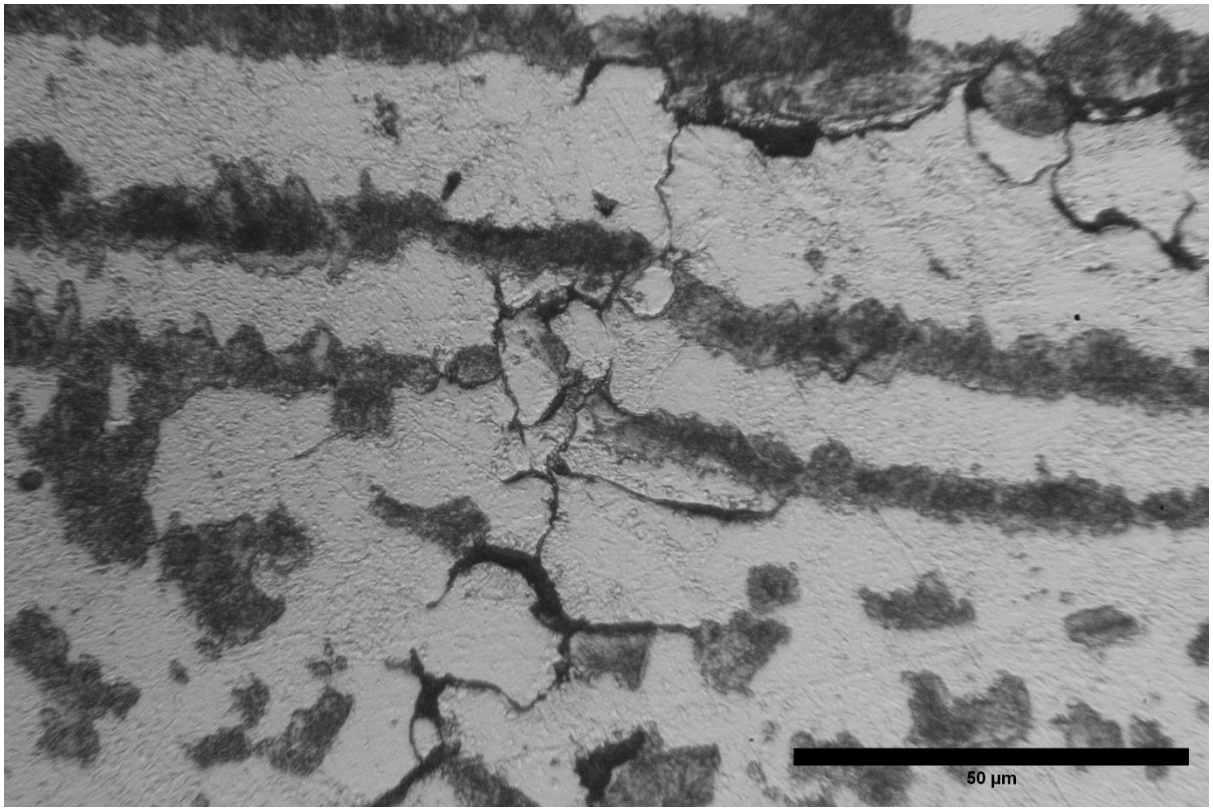

Figure 23.Intergranular fissure propagation perpendicular to the direction of pearlite banding.

The number of cracks diminishes significantly near the external surface of the equipment, in opposition to the internal surface which shows signs severe HTHA damage.

Decarburization in the vicinity of the main crack is enhanced. With the crack formation additional surfaces for surface decarburization are created. In some regions, veins appear, apparently due to the influence of residual stresses, possibly due to welding (Figure 24).

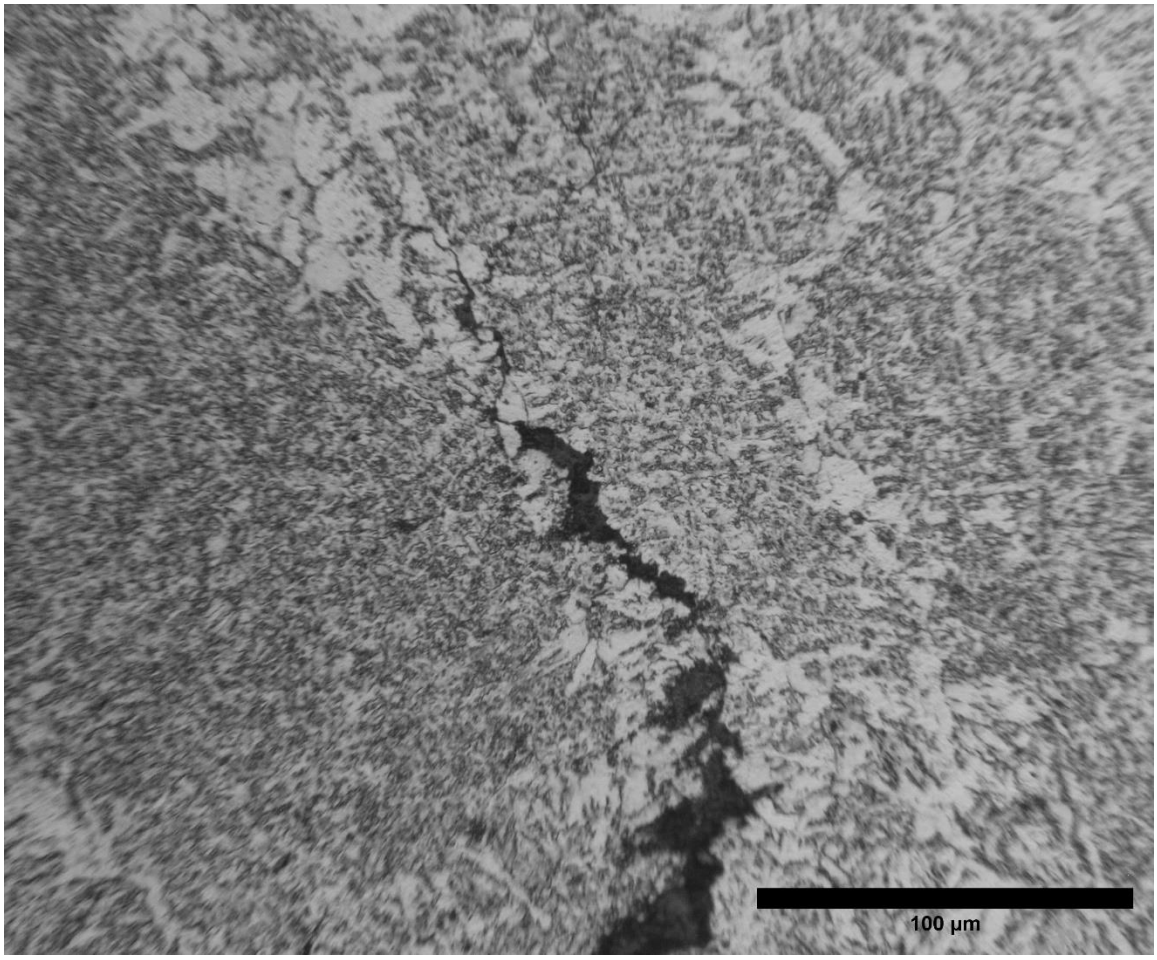

Figure 24. Decarburization of the banks of the main crack.

5.2.3 Microhardness measurement

Microhardness measurement revealed that the base metal's hardness is in between 187,6 and 196,9 $HV_{0.3}$. On the HAZ side, the hardness is within the range of 220,5-245,1 $HV_{0.3}$. Close to the main crack, the hardness is between 204,5-216 $HV_{0.3}$, possibly due to surface decarburization taking place in the area.

5.3 Fractographic description

The main crack was cracked open revealing the crack surface. SEM examination of the crack surface indicated severe HTHA damage. Cracks are evident on the grain boundaries, in the form of intergranular micro-fissuring, as the red arrows indicate. Micro fissuring was previously observed through the optical microscopy examination of the specimen.

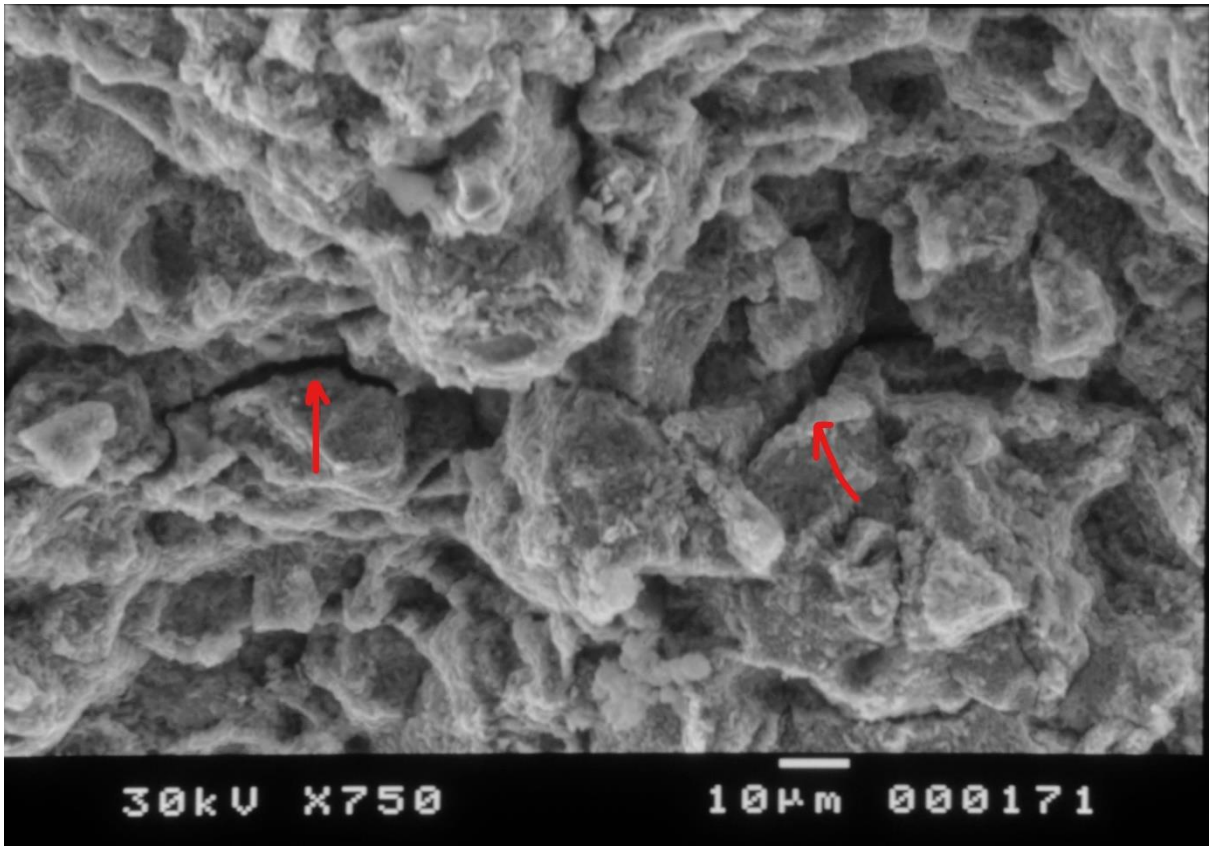

Figure 25. Intergranular fissuring evidence.

Also, voids can be detected on the grain facets, as the red arrows in (**Error! Reference source not found.**) indicate.

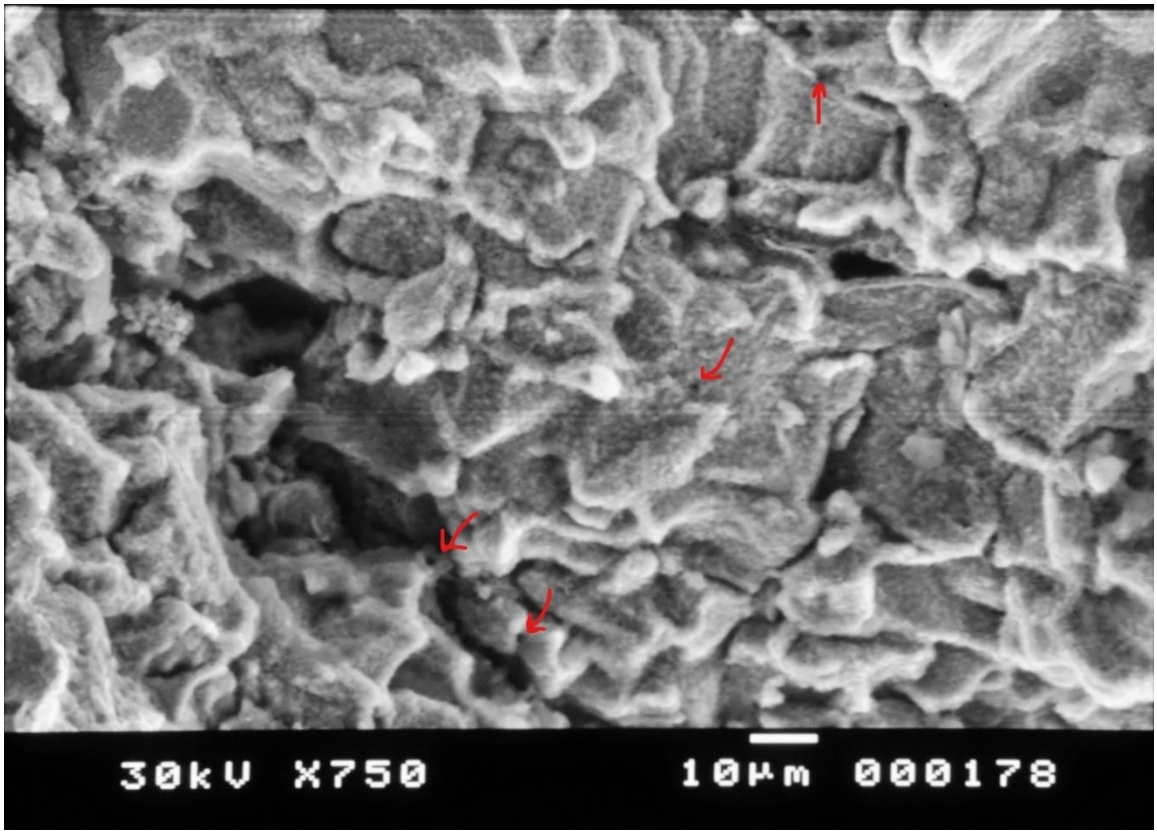

Figure 26. Voids on the grain boundary facets.

6. Conclusions

6.1 Specimen examination evidence discussion

- A crack, of 0.5m, covers a section of the carbon steel heat exchanger M-9210 and spreads from the internal surface along the thickness of the material.

- According to the operational information the heat exchanger was operating far above the limits set by the Nelson Curves for non-Post Weld Heat Treated carbon steel, and the Post Weld Heat Treated. Surpassing the limit set by the Nelson Curves, makes it highly possible for HTHA to appear. Carbon steel is also the most susceptible material for this type of attack. The operating limits, for non-PWHT carbon steel, are indicated by the lowest curve, as shows the red arrow.

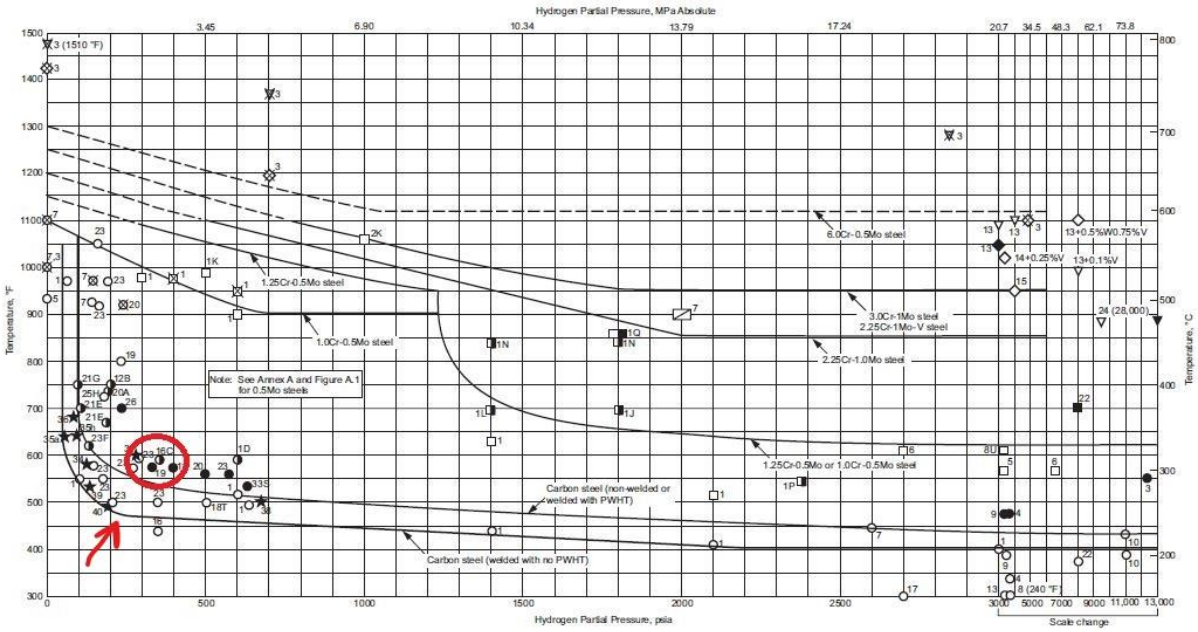

Figure 27. Area of operating conditions for exchanger M-9210

- The metallographic examination of a specimen, coming from the heat exchanger M-9210, revealed that the responsible failure mechanism is High Temperature Hydrogen Attack. The main propagated from the hydrogen rich internal surface of the exchanger tube and thinned as it propagated within the tube's thickness. Indications of intense decarburization, on the internal surface and the banks of the main crack, and intergranular grain boundary separation and intergranular fissuring led to this assumption.

- The material optical examination revealed a ferrite-pearlite microstructure. The cementite carbides of the pearlitic matrix, probably dissolve, to provide carbon which reacted with the dissolved hydrogen and led to methane creation. Decarburization took place in the vicinity of the main crack, as pearlite dissolution reveal in the metallographic examination.

- Sem examination reveals the presence of bubbles/blisters on the grain boundary facets. Methane filled voids' appearance is characterized as the initial stage, referred to as incubation stage, indicating HTHA attack. As long as there is hydrogen diffusion and carbide dissolution, supplying the material with carbon, methane blisters continue to form, ensuring continuation of the HTHA mechanism. The main crack initiates at the internal surface of the equipment, where the environment is rich in hydrogen.

- The main crack propagated due to intergranular fissuring. Voids and micro-cracks separating the grain boundaries, joined to form larger ones. The main crack, causing final failure, was the result of micro-cracks/fissures coalescence.

- The main crack location is in the HAZ and BM border region of the weld. In some sections, mainly in the conjunction of the double V weld, the crack abruptly changes direction, from vertical becomes parallel to the thickness The residual stresses, created from the welding procedure, since the equipment was not heat treated, assisted crack propagation and grain boundary separation. The existing residual stresses of the weld accelerated the damage mechanism expansion.

- The main crack formation facilitated the diffusion of hydrogen to the interior of the material resulting to the formation of more fissures and surface decarburization on the banks of the main crack. The internal surface of the equipment was also decarburized, probably because of immediate contact with hydrogen-rich environment. Although surface decarburization is a minor problem, increasing hydrogen diffusion rates, in the steel, accelerates the damage rate.

- Banding in the internal surface of the equipment, created during manufacturing, facilitates fissure spreading, as it creates an easy path for the micro-cracks to expand and branch out.

6.2 Prevention and Evaluation Methods Discussion

- Petroleum refineries and plants continue to be heavily burdened by the HTHA damage and the despite the existence of the Nelson curves, there is constant need for their evaluation due to accidents occurring below the settled safe limits. The need to gather accurate information for further investigation and prevention of HTHA is rising. There should be careful monitoring of the operating and fouling conditions of equipment by every relating company. Concentration of analytical data further sheds light to the conditions under which HTHA may appear and adds awareness to the directly affected companies. Monitoring instruments on the shell internal surface can update on real time temperatures reached.

- Monitoring methods of, which do not obstruct operation of equipment are suggested. Monitoring can be used to calculate changes in operating pressures and temperatures, that affect HTHA susceptibility [14]. One monitoring technique is AET. For the challenging part of weld inspections TOFD monitoring can be the non-intrusive method used. Both methods are described in the API contents section.

- Manuals, such as the API, should be advised for better understanding of the possible methods to evaluate equipment. Evaluation for HTHA damaged equipment should be conducted by specialists, who carefully choose the proper testing mechanism and are familiar with the signals it produces and their translation. Non-destructive evaluation methods are preferable, such as AUBT together with a velocity ratio analysis and a power spectrum analysis or WFMT.

- Cladding can be used for the obstruction of hydrogen diffusion in the metal. However, cost should be taken into consideration since the equipment surface is usually wide and cladding expensive, covering the whole equipment may be unprofitable.

- High-alloyed steels offer better damage resistance than low alloyed ones and carbon steel, PWHT and not. Due to the creation of stable carbides the creation of methane bubbles is restricted, as carbon is bound from reacting with hydrogen. The Nelson Curves and the API suggest the utilization of Chromium and Molybdenum alloyed steels. Highly alloyed steels in Cr and Mo, even though pricier, show better resistance and mechanical strength. The Nelson Curves can be used for material selection. However, the operating characteristics should be carefully considered.

- All already operating equipment susceptible to HTHA, especially made of carbon steel or low alloyed steel, should be evaluated for fitness for service. Outages should be carefully investigated and not normalized, because they retreat under certain conditions and are no cause, yet, of failure.

To conclude, chances of HTHA can be effectively reduced by understanding the phenomenon through essential study and by following a careful plan during equipment selection and monitoring. Safety of the employed staff, and safety and life prolongation of the equipment should be the basic concerns of every company.

7. REFERENCES

[1] G. N. Haidemenopoulos και A. D. Zervaki, 'FAILURE ANALYSIS INVESTIGATION OF EXCHANGER M-9210'.

[2] American Petroleum Institute, 'The Technical Basis Document for API RP 941'.

[3] D. Pandelis, G. N. Haidemenopoulos, και B. I. Papazoglou, *Welding Science*.

[4] R. E. Allen, 'ANALYSIS OF THE EARLY STAGES OF THE HYDROGEN ATTACK OF STEEL', σ. 13.

[5] MISTRAS Group, 'HTHA | High Temperature Hydrogen Attack'.

[6] B. Saba, 'Evaluation of mechanical fitness for service of high temperature hydrogen attacked steels', Master of Science in Mechanical Engineering, Louisiana State University and Agricultural and Mechanical College, 2003. doi: 10.31390/gradschool_theses.3883.

[7] C. Allevato, 'Utilizing acoustic emission testing to detect high-temperature hydrogen attack (HTHA) in Cr-Mo reformer reactors and piping during thermal gradients', *Procedia Eng.*, τ. 10, σσ. 3552–3560, 2011, doi: 10.1016/j.proeng.2011.04.585.

[8] M. T. Bodden Connor και Christopher D. Barrett, 'Introduction of Molecular Dynamics for HTHA and a Review Article of HTHA'.

[9] K. Poorhaydari, 'A Comprehensive Examination of High-Temperature Hydrogen Attack—A Review of over a Century of Investigations', *J. Mater. Eng. Perform.*, τ. 30, τχ. 11, σσ. 7875–7908, Νοεμβρίου 2021, doi: 10.1007/s11665-021-06045-z.

[10] K. Poorhaydari, 'Failure of a hydrogenerator reactor inlet piping by hightemperature hydrogen attack'.

[11] R. J. Mostert, T. W. Mukarati, C. C. E. Pretorius, και V. M. Mathoho, 'A constitutive equation for the kinetics of high temperature hydrogen attack and its use for structural life prediction', *Procedia Struct. Integr.*, τ. 37, σσ. 763–770, 2022, doi: 10.1016/j.prostr.2022.02.007.

[12] M. L. Martin, M. Dadfarnia, S. Orwig, D. Moore, και P. Sofronis, 'A microstructure-based mechanism of cracking in high temperature hydrogen attack', *Acta Mater.*, τ. 140, σσ. 300–304, Νοεμβρίου 2017, doi: 10.1016/j.actamat.2017.08.051.

[13] E. E. Fletcher και A. R. Elsea, *THE EFFECTS OF HIGH - PRESSURE, HIGH - TEMPERATURE HYDROGEN ON STEEL*.

[14] D. J. Benac και P. McAndrew, 'Reducing the Risk of High Temperature Hydrogen Attack (HTHA) Failures', *J. Fail. Anal. Prev.*, τ. 12, τχ. 6, σσ. 624–627, Δεκεμβρίου 2012, doi: 10.1007/s11668-012-9605-x.

[15] W. Sharp και R. Mostert, 'Practical Experience in the early Detection and Assessment of Vessels with HTHA Degradation', σ. 8.

[16] A. Askari και S. Das, 'Practical numerical analysis of a crack near a weld subjected to primary loading and hydrogen embrittlement', *J. Mater. Process. Technol.*, τ. 173, τχ. 1, σσ. 1–13, Μαρτίου 2006, doi: 10.1016/j.jmatprotec.2004.12.005.

[17] J. M. Brear και J. M. Church, 'Technical Basis For API Publication 941 ('Nelson Curves')'.

[18] M. Bharadwaj, 'Studies of High Temperature Hydrogen Related Damage in Welded Carbon Steel Components used in Refineries', σ. 237.

[19] J. R. Thygeson και M. C. Molstad, 'High Pressure Hydrogen Attack of Steel.', *J. Chem. Eng. Data*, τ. 9, τχ. 2, σσ. 309–315, Απριλίου 1964, doi: 10.1021/je60021a056.

[20] G. N. Haidemenopoulos, *Natural Metallurgy*.

[21] A. Reizis, 'MICROSTRUCTURE STUDY OF LOW ALLOY STEEL AFTER THE APPLICATION OF A RAPID THERMAL CYCLE', National Technical university of Athens.

[22] U.S. CHEMICAL SAFETY AND HAZARD INVESTIGATION BOARD, 'INVESTIGATION REPORT, CATASTROPHIC RUPTURE OF HEAT EXCHANGER, TESORO ANACORTES REFINERY'.

[23] U.S. CHEMICAL SAFETY AND HAZARD INVESTIGATION BOARD, 'E-6600E and E-6600B Heat Exchanger Metallurgical Analysis'.

[24] Inspectioneering, LLC, 'Overview of Integrity Operating Windows (IOWs)'.

[25] H. Malekmohammadi, ‘A review on High Temperature Hydrogen Attack (HTHA) damage mechanisms, comparison and introduction of methods applicable for t’, σ. 11, 2008.
[26] N. Trimborn, ‘Detecting and Quantifying High Temperature Hydrogen Attack (HTHA)’, σ. 4.
[27] J. Brightling και S. Shapcott, ‘Risk Reduction Projects Combating High Temperature Hydrogen Attack’, σ. 10, 2018.
[28] Laboratory Testing Inc., ‘MAGNETIC PARTICLE INSPECTION’, 2022.
[29] WELDING ANSWERS, ‘What is Post Weld Heat Treatment (PWHT)?’
[30] D. Eliezer, ‘High-temperature hydrogen attack of carbon steel’, *J. Mater. Sci.*, τ. 16, τχ. 11, σσ. 2962–2966, Νοεμβρίου 1981, doi: 10.1007/BF00540300.